

Acknowledgements

After a 5 year journey, another chapter comes to its end. What once started as the academic journey of an inexperienced and unknowing boy now ends with the writing of this thesis by a still, but less, inexperienced boy. Because during this period the first thing you learn is that in science, you never stop learning. Although it had its ups and downs, I never regretted my choice of pursuing a career in science. As a great mind once said “Success is not the key to happiness. Happiness is the key to success. If you love what you are doing, you will be successful”. I learned a lot of things and got to know many new people. But this thesis is not the end, it is only the beginning of a new and greater adventure. One in which I hope to become an even more skilled and critical scientist.

However, because science is not a job done by oneself but revolves around teamwork, I would like to take this opportunity to show my gratitude to some people:

First of all, I would like to thank dr. Ethirajan Anitha, promotor of my masterthesis. Through the past year she has thought me to look critical at my own results, that determination is a much needed quality for a scientist and that you never stop learning. She always pushed me to expand my limits and become a better scientist. Also, she coached me during my experimental work and supported me in writing this thesis. And last but not least, she always showed a large amount of patience.

I also would like to thank my co-promotor, Professor Junkers Thomas, for sharing his knowledge during scientific discussions and for his input and interest in my master thesis. I am also grateful to Professor Hellings Niels, who provided me with the opportunity to conduct cell experiments at BIOMED. Also my thanks to all three of them for their input in my BOF application. I also want to acknowledge Professor Manca Jean, my second referee, for his interest in my work and for making time for me despite his highly occupied schedule.

The following people are gratefully acknowledged for their technical support during my thesis. First, dra. D’Olieslaeger Lien for the TEM imaging and her guidance as my daily supervisor. Dra. Kayte Ranieri for the synthesis of the chemical compounds and her guidance in the chemistry lab. Dra. Neomy Zaquen for the synthesis of the MDMO-PPV. Dr. Linn Baeten for her scientific input. Dr. Boelen Ellen for introducing me to everyone at BIOMED and providing me with the necessary equipment. Wauterickx Katrien for all the time she spent on arranging the things I needed. Dra. Hilken Petra for lending me some of her precious cells. Dr. Bogie Jeroen, for helping me with the FACS experiments. Dr. Smisdom Nick and drs. Notelaers Kristof for providing me with technical and scientific support regarding the confocal microscopy. Dra. Timmermans Silke for her help with the epifluorescence microscope. Christel Willems, Johnny Baccus, Hilde Pellaers and Erik Thoonen for their technical support. Also thanks to the master students Vanoppré Wouter and Van der Auwera Jo for their help during their junior internship. And also thanks to all the other people on IMO and BIOMED for providing a pleasant environment to work in.

I would also like to thank my parents for their support during my whole educational career and for providing me with the opportunity to pursue my dreams. And last but not least, I would like to thank Hannelore, for her endless support, scientific input and patience during the last months.

Table of Contents

Acknowledgements	i
Table of Contents	ii
Abbreviations	iv
Abstract	v
Nederlandse Samenvatting	vi
1. Introduction.....	1
1.1 General Overview.....	1
1.2 Theoretical Background.....	3
1.2.1 Surface Functionalization of Polymeric Nanoparticles <i>via</i> Combination of Nitron Chemistry and Miniemulsion Technique.....	3
1.2.2 Bioimaging using Fluorescent π -conjugated Polymer Nanoparticles.....	7
2. Materials & Methods	11
2.1 Materials.....	11
2.1.1 Surface Functionalization of Polymeric Nanoparticles <i>via</i> Combination of Nitron Chemistry and Miniemulsion Technique.....	11
2.1.2 Bioimaging using Fluorescent π -conjugated Polymer Nanoparticles.....	11
2.2 Methods	12
2.2.1 Surface Functionalization of Polymeric Nanoparticles <i>via</i> Combination of Nitron Chemistry and Miniemulsion Technique.....	12
2.2.2 Bioimaging using Fluorescent π -conjugated Polymer Nanoparticles.....	14
2.2.3 Characterization Methods.....	17
3. Results & Discussion.....	21
3.1 Surface Functionalization of Polymeric Nanoparticles <i>via</i> Combination of Nitron Chemistry and Miniemulsion Technique	21
3.1.1 Determination of Partition Coefficients of PBN and NHS Nitron	21
3.1.2 Synthesis of polyDVB Nanoparticles with ESCP and Miniemulsion Technique.....	21
3.1.3 Grafting From Approach using PBN Functionalities	22
3.1.4 Grafting To Approach using NHS Nitron Functionalities	24
3.2 Bioimaging using Fluorescent π -conjugated Polymer Nanoparticles.....	26
3.2.1 Characterization of the Fluorescent Materials.....	26
3.2.2 Characterization of the Fluorescent NPs.....	28
3.2.3 Nanoparticle-cell Interaction Studies.....	32
4. Conclusion & Outlook.....	37
References.....	39

Abbreviations

NPs	Nanoparticles	AgNO₃	Silver nitrate
ESCP	Enhanced spin capturing polymerization	Al₂O₃	Aluminum oxide
DVB	Divinylbenzene	P/S	Penicillin/streptomycin
PBN	α -Phenyl-N- <i>t</i> -butyl nitron	HC	Hydrocortisone
NIPAAm	N-isopropylacrylamide	MTT	Methylthiazolyldiphenyl-tetrazolium bromide
LCST	Low critical solution temperature	PFA	Paraformaldehyde
MRSA	Methicillin-resistant Staphylococcus Aureus	CHCl₃	Chloroform
NHS	N-hydroxysuccinimide	DMSO	Dimethyl sulfoxide
IgG	Immunoglobuline G	FCS	Fetal calf serum
MDMO-PPV	Poly[2-methoxy-5-(3',7'-dimethyloctyloxy)-1,4-phenylene-vinylene]	EGF	Epidermal growth factor
PPV	Poly(p-phenylene vinylene)	DAPI	4',6-diamidino-2-phenylindole
PLLA	Poly-L-lactide	PBS	Phosphate buffered saline
K_B	Boltzmann constant	TEM	Transmission electron microscopy
T	Temperature	DLS	Dynamic light scattering
χ	Interaction parameter	IR	Infrared
φ	Volume fraction	EDX	Energy dispersive X-Ray analysis
N	Number of molecules	UV-Vis	ultraviolet-Visible
FDA	Food and drug administration	FACS	Fluorescence activated cell sorting
Fe₃O₄	Magnetite	D	Diffusion coefficient
HMEC-1	Human microvascular endothelial cell	η	Solvent viscosity
QDs	Quantum dots	ATR	Attenuated total reflectance
CdSe/ZnS	Cadmium Selenide/Zinc Sulfide	FTIR	Fourier transform infrared spectroscopy
IMO	Institute for materials research	A	Absorption
PRDG	Polymer reaction design group	ϵ	Absorption coefficient
SDS	Sodium dodecyl sulfate	l	path length
NaBH₄	Sodium borohydride	C	Concentration
AIBN	2,2'-Azobis(2-methyl-propionitrile)	PDI	Polydispersity
THF	Tetrahydrofuran	rpm	Revolutions per minute
DMF	Dimethylformamide		

Abstract

Multifunctional nanoparticles combine several properties into one stable construction, providing a very promising tool for the medical world. For example, surfaces can be functionalized for recognition or stealth purposes, materials can be encapsulated for magnetic guidance or the release of (bio-) active substances and imaging agents can be loaded, all at the same time. However, converting these theoretical designs into a usable application is a multi-step process that usually costs a lot of time, effort and money. It is therefore no surprise that a lot of research is ongoing in developing new methods and designing new materials to shorten the process. The aim of this thesis is to advance the research of designing multifunctional nanoparticles.

The first part of the thesis covers the production of surface functionalized polymer nanoparticles. These particles are made by combining the miniemulsion technique with enhanced spin capturing polymerization and their size is tunable from 50 to 500 nm. The combination of these techniques for the synthesis of nanoparticles has not been reported before in literature and provides a faster way to insert functional groups into nanoparticles than many currently used methods. By employing different nitrones in the polymerization reaction of the monomer divinylbenzene, certain functionalities can be introduced *in situ* on the surface of the nanoparticles. Two different nitrones, namely α -phenyl-N-*t*-butyl and n-hydroxysuccinimide, synthesized by the Polymer Reaction Design Group of the Institute for Materials Research, are used in this thesis. With the PBN nitron, a 'grafting from' approach is employed to polymerize a shell of thermoresponsive polyNIPAAm onto the surface, creating a composite (organic/organic) buildup. The composite nanoparticles are then used to incorporate silver nanoparticles into their shells, generating a composite-hybrid (organic/organic-inorganic) buildup. These nanoparticles have the possibility to be used for medical coatings due to the anti-bacterial, -viral and -fungal properties of the silver nanoparticles. With the NHS nitron, a 'grafting to' approach is employed to bioconjugate gold labeled IgG antibodies using the activated NHS ester present on the nanoparticle surface. These activated NHS esters can be used to couple any biologically relevant molecule containing an amine group to the nanoparticle.

The second part of the thesis covers the production of fluorescent polymer nanoparticles. These particles are made with the semiconducting polymer MDMO-PPV, synthesized *via* the sulfinyl route by the Polymer Reaction Design Group, by combining the solvent/evaporation technique with the miniemulsion technique. The use of MDMO-PPV for fluorescent nanoparticle imaging systems has not yet been documented in the literature before. Multifunctionality is introduced in this system by synthesizing magnetite encapsulated MDMO-PPV hybrid nanoparticles and magnetite encapsulated MDMO-PPV/PLLA composite-hybrid nanoparticles. The encapsulation of magnetite provides a way to localize the particles in the human body by applying a magnetic field. The PLLA, a biodegradable FDA approved polymer can be used to load (bio-) active substances. Since it is the first time that these kind of nanoparticles are synthesized for bioimaging, cell experiments are performed in BIOMED, in cooperation with the Immunology group to study possible cytotoxic effects and the cellular uptake of the particles using HMEC-1 cells.

Nederlandse Samenvatting

Multifunctionele nanodeeltjes combineren verschillende eigenschappen tot een stabiele constructie waardoor ze een zeer interessante werktuig vormen voor de medische wereld. Zo kunnen tegelijkertijd oppervlakte gefunctionaliseerd worden en materialen binnenin opgeslagen worden. Het omzetten van zulke modellen naar een toepassing is echter een tijdrovend en duur proces dat meerdere stappen beslaat. Aldus, vindt er veel onderzoek plaats naar het zoeken van nieuwe materialen en methoden die dit proces kunnen vergemakkelijken. Het doel van deze thesis is om dit onderzoek vooruit te helpen.

Het eerste deel van deze thesis beslaat de synthese van gefunctionaliseerde polymere nanodeeltjes, door de miniemulsie techniek te combineren met *enhanced spin capturing polymerisation*. De combinatie van deze technieken levert een snelle manier voor het introduceren van functionele groepen in het oppervlak van nanodeeltjes en is tot op heden nog nergens vermeld in de literatuur. Door verschillende nitronen te gebruiken in de polymerisatie van het monomeer divinylbenzeen kunnen bepaalde functionaliteiten *in situ* geïntroduceerd worden. In deze thesis is er gebruik gemaakt van de nitronen α -Phenyl-N-*t*-butyl (PBN) en n-hydroxysuccinimide (NHS), gesynthetiseerd door de Polymer Reaction Design groep van het Instituut voor Materiaalonderzoek. In het geval van PBN is er gebruik gemaakt van een 'enten vanaf' aanpak om een polymeer schil bestaande uit thermogevoelig polyNIPAAm te synthetiseren op het oppervlak, resulterend in een samengestelde opbouw (organisch/organisch). Deze samengestelde deeltjes zijn vervolgens gebruikt voor het immobiliseren van zilver nanodeeltjes, wat een samengestelde-hybride opbouw tot gevolg heeft (organisch/organisch-anorganisch) welke gebruikt kan worden voor medische coatings. In het geval van NHS nitrone is er een 'enten aan' aanpak aangewend om goud gelabelde antilichamen vast te hechten aan het oppervlak. Deze geactiveerde NHS esters kunnen gebruikt worden om elk biologisch relevant molecuul met een aminegroep aan te hechten aan een nanodeeltje.

Het tweede deel van de thesis omvat de productie van fluorescerende polymere nanodeeltjes opgebouwd uit het halfgeleidend polymeer MDMO-PPV, gesynthetiseerd *via* de sulfinyl route door de Polymer Reaction Design groep. De synthese omvat een combinatie van de solvent/evaporatie techniek en de miniemulsie techniek. Het gebruik van deze fluorescente MDMO-PPV nanodeeltjes voor visualisatiedoeleinden is nog niet beschreven in de literatuur. Multifunctionaliteit wordt geïntroduceerd door de synthese van magnetiet bevattende MDMO-PPV hybride nanodeeltjes en magnetiet bevattende MDMO-PPV/PLLA samengestelde-hybride nanodeeltjes. Met magnetiet kunnen de deeltjes naar specifieke locaties getransporteerd worden in het lichaam. PLLA is dan weer een biodegradeerbaar polymeer dat gebruikt kan worden voor het vrijzetten van bioactieve substanties. Aangezien dit de eerste keer is dat deze nanodeeltjes worden gesynthetiseerd met *in vivo* beeldvorming als doel, worden er cel studies uitgevoerd worden om de cytotoxiciteit en cellulaire opname na te gaan. Deze studies vinden plaats op HMEC-1 cellen in BIOMED, in samenwerking met de immunologie vakgroep.

1. Introduction

1.1 General Overview

An old dream of natural science is the deliberate and local manipulation of matter on the atomic or molecular scale. The origin of this vision dates back to 1959 when Nobel Laureate Richard Feynman held his famous and visionary lecture “There is plenty of room at the bottom” at the annual meeting of the American Physical Society (1). It was from the concepts of this talk that the field of nanoscience arose. Although considered a modern branch of science, the use of nanotechnology predates back to the 9th century where gold and silver nanoparticles were already used by Mesopotamian artisans to create a ‘glittering effect’ in pots (2). However, with recent advancements such as the invention of atomic force microscopy, transmission electron microscopy and dynamic light scattering, nanotechnology has reached a point where it is considered to be the future for all technologies.

One of the famous structures developed in this field is the nanoparticle, a particle with a tunable size in the nanometer range, which is in the same dimension as antibodies, membrane receptors, proteins and other biomolecules. It is the combination of this biomimetic property with a high surface to volume ratio and the ability to modify the features of the particle that has caused a significant rise in interest in the research of nanoparticles for biomedical applications during the last decade. The integration of nanotechnology with medical sciences has opened tons of new possibilities and due to the exponential increase in research in this topic, the field is constantly evolving, which has allowed for a better understanding of molecular biology. This has provided medicine with novel and faster methods to study, diagnose and treat diseases for which the targeting was previously size restricted. Despite these benefits which nanoparticles have rendered, some applications like *in vivo* real-time monitoring of cellular events, specific action site targeting and targeted drug delivery remain challenging. Multifunctional nanoparticles could be used to improve the characteristics of monofunctional designs and surmount these problems. These multifunctional nanoparticles use a combination of various properties to form a stable construct. A particle can for example be loaded with a drug, functionalized with recognition groups and labeled with an imaging agent. However, converting such theoretical designs to practical and usable applications is an elaborate multi-step process that requires a great amount of time, effort and money. Because of this, new techniques or materials that can circumvent or simplify the multistep process are highly requested. Therefore, the goal of this thesis was to further the research for designing multifunctional nanoparticles. The thesis is divided into two parts, each focusing on a different aspect of introducing multifunctionality in nanoparticles. The first part covers the development of a new method to functionalize nanoparticles in an efficient and convenient way through *in situ* functionalization. The second part comprises the use of a new material to improve the bioimaging characteristics of nanoparticles. (3)

The first part of this master thesis dealt with surface functionalization of nanoparticles, which is a requirement for almost every biomedical application. The reason it is so important is because surface functionalization determines the interaction of the nanoparticle with the environment. It are these interactions that determine the colloidal stability, the target specific delivery and the cellular uptake of the nanoparticles. Therefore, it is necessary to have functional groups present on the surface which enable attachment of the required moieties. Most of the nanoparticle materials, like gold and iron oxide, to which relevant groups can be coupled conveniently by for example chemisorption, are inorganic. The direct coupling occurs due to affinity between the inorganic surface and a certain functional group, for example thiol-groups with a gold surface. However, these bonds undergo dynamic binding and unbinding processes resulting in the possibility of losing the coupled structures by extensive washing or mass action by another structure (4). This can compromise the stability of the nanoparticles. Also, scientific discussion is still ongoing regarding possible cytotoxic effects of these materials (5, 6). To overcome the cytotoxicity issue, polymers can be used. The resulting polymeric nanoparticles are often biocompatible, non-immunogenic and non-toxic (7). Unfortunately, functional groups used for surface functionalization are absent in most polymers. There are two main concepts for introducing these surface functional groups in nanoparticles: the post-synthesis and *in situ* method. Post-synthesis functionalization is a method used to introduce functional groups on already formed nanoparticles, while *in situ* functionalization introduces these groups during the synthesis of the nanoparticles. The first introduction method is complex, inefficient and time consuming (8, 9). Therefore, a new method for introducing surface functionalities *in situ* was explored in this thesis, namely the combination of the miniemulsion technique and enhanced spin capturing polymerization. This feature was already proven for the synthesis of microspheres but has not yet been transferred to the synthesis of nanoparticles (10). By combining these two methods a water-based dispersion of alkoxyamine functionality containing polymer nanoparticles is made in a minimum amount of time and effort. On one side the end-product is free of organic solvents, making it environmentally and economically favorable and on the other side the nanoparticles already contain a functional group. This *in situ* functionalization thus removes the need for classical post modification procedures associated with the use of catalysts or high temperatures required for ligation reactions. Thus apart from being time saving, a one-pot synthesis averts contamination of particles, tedious washing procedures and insufficient grafting densities. The resulting functionalities can be used for incorporation of other polymers, inorganic materials or both and for attachment of target recognizing groups onto the surface. In this work, surface functionalized nanoparticles synthesized with different nitrones were used for *grafting from* and *grafting to* approaches to form composite/hybrid nanoparticles.

The second part of this thesis dealt with the design of nanoparticles for bioimaging. The possibility of imaging nanoparticles is of importance since it enables their use in a “find, fight, follow” concept, called theranostics. It allows for studying the development of the disease and tracking the progress of the therapy at the same time (11). Also, fundamental aspects of cell-nanoparticle interactions, cellular uptake of nanoparticles and the underlying mechanisms can be explored (12, 13). One of the extensively employed techniques to aid optical imaging is fluorescence labeling. However, the currently used organic fluorophores are not photostable and have a low intensity (3). Their fluorescent yield is known to fade in less than one minute and dye bleaching puts a restriction on their use in applications (11). Next to this, fluorescence proteins and bioluminescence system applications are limited due to the fact that they cannot be optimized in multicolor assays. A solution

presented in literature is the use of inorganic quantum dots, nanostructures that are zero dimensional relative to bulk and resistant to photobleaching and photo, chemical and metabolic degradation (14). Also, they possess a high quantum yield, resulting in the possibility to detect multiple markers simultaneously. They have a size- and composition tunable emission, a broad absorption spectrum and a narrow emission spectrum. However, the selenides and sulfides used are cytotoxic and can therefore only be used for *in vitro* purposes (11). An additional disadvantage is that quantum dots undergo degradation *in vivo*, leading to quenching of the fluorescence (11).

In this work, a new potentiality for the visualization of nanoparticles was investigated, namely the synthesis of nanoparticles built up of a semiconducting polymer. As compared to the first part of the thesis where polymer particles were formed using respective monomer, here, preformed polymers were used for the nanoparticle formation by employing a combination of the miniemulsion and solvent evaporation technique. The conjugated polymer is built up of a π -conjugated backbone consisting of unsaturated units and is functionalized with solubilizing substituents (15). They hold great promise due to their comparatively low cost, resulting from inexpensive manufacturing methods. They also have a strict correlation between structural and physical characteristics, allowing for the tuning of their properties by chemical modifications (16). Another characteristic feature is that they have a higher brightness, photostability and absorption cross-section than the currently used molecular dyes (17, 18). The conjugated polymer used here was a common PPV derivative, poly[(2-methoxy-5-(3', 7', -dimethyloctyloxy))-1,4 phenylene vinylene], which was synthesized at the Institute for Materials Research by the polymer reaction design group. Although a highly intriguing material for bioimaging, not much is known about its cytotoxicity. Therefore, this thesis sheds light on the biocompatibility as well as the cell-uptake of fluorescent nanoparticles built up of this polymer. Additionally, multifunctional hybrid nanoparticles with interesting morphologies were designed, using different material combinations with MDMO-PPV as a main building block, and studied for cytotoxicity. The cell experiments were executed at BIOMED in collaboration with the immunology group of Prof. dr. Hellings.

1.2 Theoretical Background

1.2.1 Surface Functionalization of Polymeric Nanoparticles *via* Combination of Nitron Chemistry and Miniemulsion Technique

As stated previously, functionalities can be introduced into polymeric nanoparticles (NPs) using a technique called enhanced spin capturing polymerization (ESCP). ESCP is a form of controlled radical polymerization in which efficient radical scavengers, nitrones, are used in the presence of the monomer and a photo- or thermal initiator. A controlled radical polymerization has the advantage that it leads to the generation of polymeric materials with tailored properties and a well-defined construction. ESCP uses the ability of nitrones to put a limit on the lifetime of propagating radicals and to induce termination by joining two macroradicals *via* two sequential spin capturing reactions (Figure 1) (19).

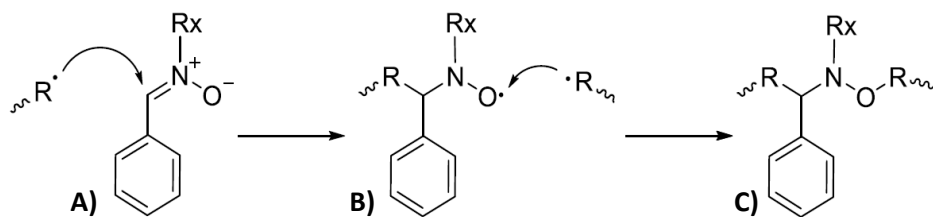


Figure 1. Simplified enhanced spin capturing polymerization mechanism. A) Formation of a macronitroxide species *via* the reaction of the nitron with a macroradical; B) Coupling of the macronitroxide to another macroradical; C) Terminated polymer chain with alkoxyamine functionality. (20)

The sequential spin capturing events take place as follows: In the first spin capturing reaction the nitron forms a macronitroxide species with a macroradical. This macronitroxide species then serves as a secondary spin quencher for another propagating macroradical, resulting in a polymer chain with an alkoxyamine function in the middle. The growing polymer chain in this thesis consists of divinylbenzene (DVB), a low-cost, commercially available monomer (Figure 2). In parallel, DVB functions as a crosslinker. The crosslinking occurs due to attachment of propagating chains to pending double bonds of other macromolecules (21). This results in particles consisting of a crosslinked network of polyDVB with alkoxyamine functionalities on both inside and outside of the particles. The ones located on the outside can be used to couple structures, like polymers or biomolecules such as peptides and proteins that have the ability to function as target recognizing structures. In addition, residual double bonds located on the surface of the particles enable a second way to modify the surface of the particles through, for instance, click chemistry approaches (22, 23).

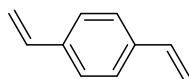


Figure 2. Chemical structure of divinylbenzene. (24)

Previously, in case of microspheres, ESCP was used in combination with precipitation polymerization (10). Precipitation polymerization starts as a homogeneous system in the continuous phase, where monomer and initiator are completely soluble. During the reaction, spherical particles grow *via* polymerization of monomers present in the solvent or by capturing newly produced chains. The capturing of new chains put a relatively fast stop to the nucleation of new particles, resulting in a narrow size distribution of the synthesized particles. During their growth, the particles undergo enthalpic precipitation, precipitation due to unfavorable polymer-solvent interactions, or entropic precipitation, which occurs because of the inability of solvent and polymer to mix freely due to chemical crosslinking of the polymer chains. (25, 26)

However, this technique cannot be transferred to the synthesis of NPs, since the following problems occur: The first drawback is the lower solid content compared to other heterogeneous polymerization methods. When the monomer concentration would be increased to get a higher solid content, the mean particle size increases too. This results in too large NPs due to an increase in the particle agglomeration rate because of the large amount of NPs present and their weak stability, and due to the higher growth rate of the generated NPs. A second drawback is the absence of a surfactant, resulting in particle coarsening due to particle collisions. This leads to the formation of irregular shaped particles and a large size distribution. The final drawback, and also one of the most

important for multifunctional NPs, is substance loading. Materials, such as water soluble drugs, which have the same polarity as the used polymer are poorly incorporable in the polymer matrix. (25-28)

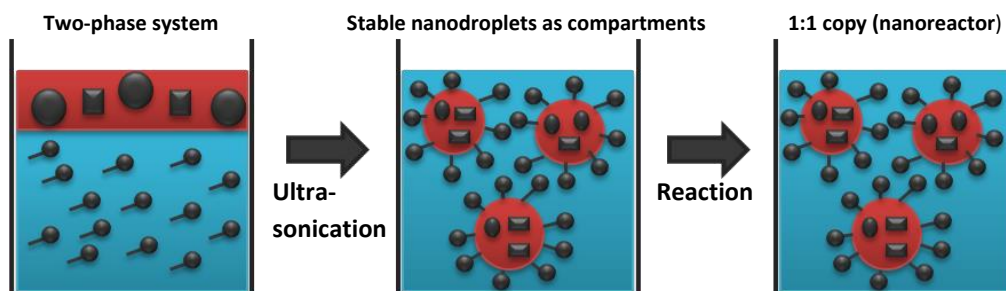


Figure 3. Miniemulsion Technique. A two phase system is made, consisting of a continuous (Phase I) and dispersed phase (Phase II). High shear forces are applied by ultrasonication to create nanodroplets and afterwards the ESCP reaction takes place creating nanoparticles. (29)

The aforementioned problems are overcome through the use of the miniemulsion technique in combination with ESCP to synthesize the NPs (Figure 3). This technique starts with a system made up of two phases, namely a dispersed and continuous phase. The continuous phase contains water and surfactant molecules, while the dispersed phase is made up of monomer dissolved in a suitable solvent containing all the materials that need to be encapsulated, like the osmotic control agent, initiator and nitrene. The surfactant molecules and osmotic control agent are used to keep the system stable during synthesis by preventing phase-separation. Surfactants are amphiphilic molecules with both a hydrophilic and hydrophobic part and their function is to reduce the interfacial tension between the dispersed and continuous phases. The osmotic control agent is a hydro-/lipophobic agent that has extremely limited/no solubility in the continuous phase, which counteracts the Laplace pressure of the droplets by generating an osmotic pressure. The two-phase system is ultrasonicated by applying high shear forces, resulting in small and stable nanodroplets dispersed in the continuous phase. Each of these droplets functions as a small nanoreactor in which the ESCP polymerization reaction takes place. After this reaction, alkoxyamine containing polymer NPs have formed inside the droplets. (30)

Grafting from approach using PBN functionalities for design of a composite-hybrid NPs:

The first nitrene used in this work is α -Phenyl-N-*t*-butyl nitrene (PBN). The generated alkoxyamine functionalities are used to integrate a polymer chain of the monomer N-isopropylacrylamide (NIPAAm) onto the surface (Figure 4). The creation of a structure, in this case a polymer, onto the surface using a functionality is called 'grafting from'. The synthesized polymer has a special property, namely thermo-responsiveness. It exhibits a low critical solution temperature (LCST) in aqueous solutions, resulting in a fast and reversible phase transition in water at a temperature of 32 °C. When this phase transition occurs the NPs become increasingly hydrophobic, resulting in particle aggregation. (10)

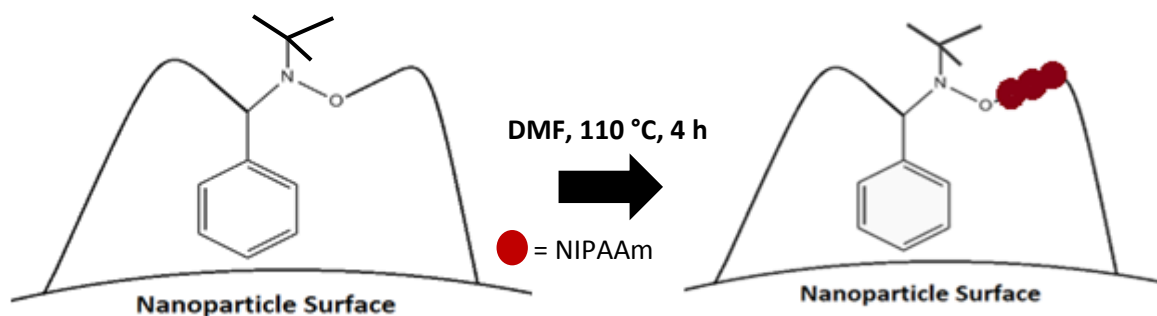


Figure 4. Grafting procedure of N-isopropylacrylamide onto the surface of alkoxyamine containing polydivinylbenzene nanoparticles. (10)

The NIPAAm network of the resulting composite NP, a particle consisting out of more than one polymer, is then used to incorporate silver NPs (Figure 5) (31). For clarity, henceforth composite and hybrid particles refer to particles comprising of only an organic and a mixture of organic/inorganic composition respectively. The disadvantage that silver NPs tend to aggregate in liquids due to their small size and large surface area is circumvented by incorporating them into the polymer network (32). Multiple studies have showed that silver NPs are non-toxic to the human body at low concentration and have broad spectrum antibacterial actions (32). The particles possess a strong biocidal effect on multiple bacterial species, including multi-resistant bacteria like Methicillin-resistant *Staphylococcus Aureus* (MRSA). The particles interact with a wide range of molecular processes in the bacteria, leading to inhibition of growth and death. Silver NPs are also known to be antiviral agents as they, for example, can inhibit the interaction between gp120 and the CD4 target cell membrane receptors, blocking HIV-1 infection (32, 33). The particles have also effects against hepatitis B, respiratory syncytial virus, herpes simplex virus type 1 and monkeypox virus (33). Another interesting feature of silver NPs is that they are antifungal agents. They show a high antifungal activity against pathogenic *Candida* spp. and yeast (34). Due to these anti-bacterial, -fungal and -viral properties the composite-hybrid NPs can be used in pharmaceutical and medical products to prevent the unwanted transmission of drug-resistant pathogens in a clinical environment.

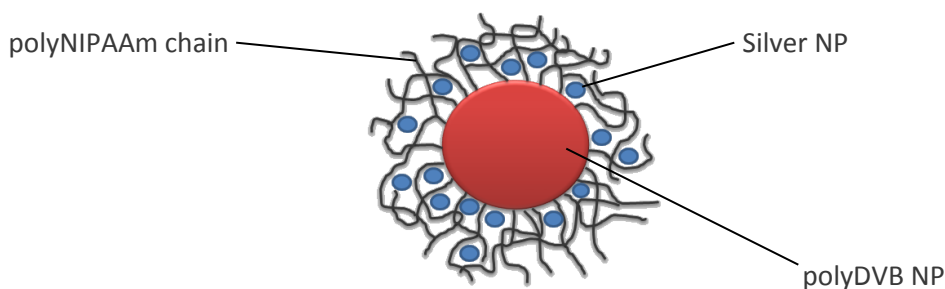


Figure 5. Silver nanoparticle loading of N-isopropylacrylamide grafted divinylbenzene nanoparticles. (31)

Grafting to approach using N-hydroxysuccinimide nitron:

The second nitron used in this work is a n-hydroxysuccinimide (NHS) nitron (Figure 6). The activated NHS ester can be used for simple covalent attachment of peptides using their primary amine (35). The attachment of preformed compounds using functionalities is called 'grafting to'. In order to show the proof of principle, bioconjugation with antibodies is performed. Due to their easy imaging properties under an electron microscope, gold NP labeled goat anti-mouse IgG antibodies are attached to the NHS group containing polyDVB NPs by formation of an amide bond.

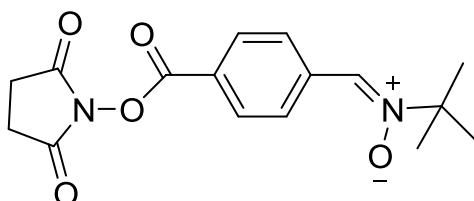


Figure 6. Chemical structure of n-hydroxysuccinimide nitron.

1.2.2 Bioimaging using Fluorescent π -conjugated Polymer Nanoparticles

In the second part of this thesis fluorescent NPs are synthesized using the organic π -conjugated semiconducting polymer poly[2-methoxy-5-(3',7'-dimethyloctyloxy)-1,4-phenylene-vinylene] (MDMO-PPV) as a building block. Also hybrid nanoparticles consisting of interesting material combination with MDMO-PPV as a major component are synthesized.

As stated before MDMO-PPV falls under the category of conjugated polymers, which are macromolecules with a main chain built up of unsaturated conjugated π -bonds (Figure 7). The coalescing of the molecular orbitals resulting from this conjugation creates a semiconductor band structure. This structure consists of a valence band, filled with electrons, and a conduction band, depleted of electrons. The energy difference between the two bands is called the band gap. When the energy of an excitation photon is high enough, depending on the band gap, the electron will jump to the conduction band leaving behind a positively charged electron hole. When the electron falls back due to coulomb attraction, a photon is emitted with a wavelength proportional to the energy of the band gap. In this way fluorescence is generated (36). Together with the other poly(p-phenylene vinylene) (PPV) derivatives it forms a class of conjugated polymers with a broad range of applications in optoelectronic devices and biosensors (37-39). PPV derivatives with backbone functionalization are very interesting as they allow better tunability of properties, especially regarding solubility, which is often a problem in wet-processing of conjugated materials. Also, by functionalization, biocompatibility/biofunctionalization can be achieved for interesting biomedical applications, i.e. biosensors or biomarkers.

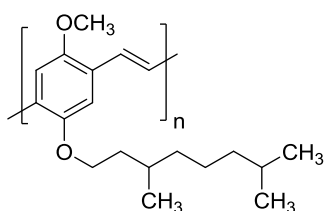


Figure 7. Chemical structure of MDMO-PPV.

The MDMO-PPV NPs are synthesized using a combination of the miniemulsion method and the emulsion/solvent evaporation technique (Figure 8). The synthesis starts with a two phase system consisting out of a dispersed phase, containing the preformed polymer dissolved in a suitable solvent which evaporates easily, and a continuous phase, containing water soluble surfactant in an aqueous solution (29). By applying high shear force, stable nanodroplets are created in which - after evaporation of the organic solvent - solid nanoparticles are formed by precipitation of the polymer chains (40).

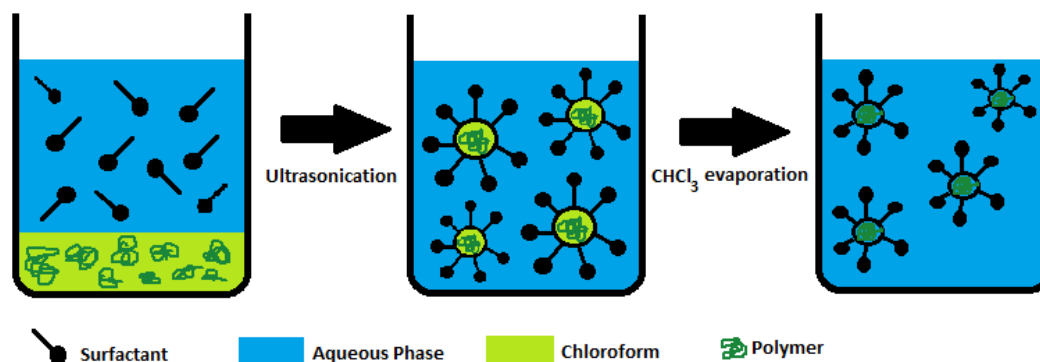


Figure 8. Combination of miniemulsion and emulsion/solvent evaporation technique. A two phase system is made, consisting of a continuous and dispersed phase. High shear forces are applied by ultrasonication to create nanodroplets and afterwards the chloroform is evaporated, creating NPs by precipitation of the polymer chains. (40)

To increase the multifunctionality of the NPs, a polymer blend of fluorescent MDMO-PPV and biodegradable poly-L-lactide (PLLA) is used to synthesize composite NPs. Since most polymers are immiscible in each other, phase separation occurs between them in the confined space of the nanodroplet upon evaporation of the solvent, resulting in NPs with a well-defined morphology (Figure 9) (41). The adopted structure is the equilibrium morphology, which is the one with minimal Gibbs free energy. The change in Gibbs free energy occurring during mixing of two immiscible polymers is calculated by the Flory-Huggins equation:

$$\Delta G_{\text{mix}} = k_B T [\chi_{12} N_1 \varphi_2 + N_1 \ln \varphi_1 + N_2 \ln \varphi_2]$$

Equation 1. Flory-Huggins equation: k_B , Boltzmann constant; T , temperature; χ , interaction parameter; φ , volume fraction; N , number of molecules.

In this equation, the volume fractions and interaction parameters are the most important parameters. Three different factors contribute to the interaction parameter: the free volume, the special interactions and the dispersion forces that are very weak. The free volume can be described as a small amount of unfilled volume, associated with the end of the polymer chain, which is dependent on the number of chain ends. Therefore, it is linked to the degree of polymerization. The special interactions, like hydrogen bonding, have also a strong influence on the value of the interaction parameter. Apart from these factors, the interaction parameter is also strongly dependent on the materials used. When chloroform is present in the nanodroplet, it is kept within the single phase region. During evaporation of chloroform, an increase in the mixture of polymers will occur inside the nanodroplet due to precipitation of the polymer chains. This will cause an exceeding of the demixing level and therefore phase separation between the polymers will occur. The

evaporation of chloroform does not only have an effect on the volume fractions in the Flory-Huggins equation but also on the interaction parameter, which increases in importance when the polymers precipitate. During the evaporation process, the polymers will phase separate into a certain morphology that depends on the used materials and volume fractions of the polymers. Therefore, the morphology can be controlled by altering the volume fractions and material combinations. (42-44)

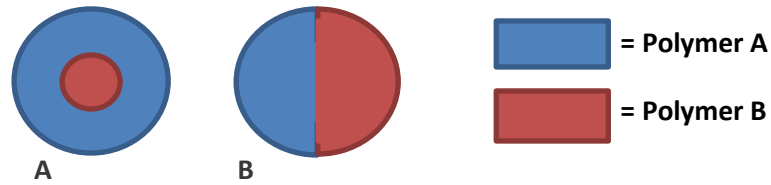


Figure 9. Nanoparticle Morphologies. A) Core-shell buildup; B) Janus buildup.

In case of MDMO-PPV/PLLA combination, a Janus like structure is formed with on one side MDMO-PPV and on the other PLLA (13). The term Janus refers to the ancient Roman god named Janus, who was believed to have two opposing faces (45). PLLA, a biodegradable polyester, is a very valuable material for biological applications. It has received FDA approval for *in vivo* use and is the most promising biodegradable synthetic polymer nowadays (46). It is already used in a wide variety of implantable medical devices, like vascular stents. It can be used to incorporate drugs or for coupling biological groups onto the particle, like for example stealth or recognition groups. This latter feature can be achieved by creating surface carboxylic acid groups by hydrolyzing PLLA, which cleaves the ester bonds (40, 47). Subsequently, biologically relevant groups can be coupled to the surface with the EDC coupling technique (13).

A final modification which is executed to increase the multifunctionality of the NPs design is the encapsulation of superparamagnetic magnetite (Fe_3O_4) particles in the polymer NPs, resulting in hybrid NPs. This is done by dispersing the magnetite particles in the dispersed phase of the miniemulsion. Two compositions are constructed in this thesis with magnetite as a building block, namely a hybrid buildup of MDMO-PPV and magnetite and one of MDMO-PPV/PLLA with magnetite. Superparamagnetism occurs when ferromagnetic substances, substances with a permanent magnetic moment, decrease to nanometer size (48). At this nanometer size the material changes from a state with multiple magnetic domains to one with a single domain and the thermal energy becomes equal to the energy needed to randomly flip the direction of the spins. This results in particles without a magnetic moment. However, these particles can still respond to an external magnetic field. This susceptibility to an external field can be exploited for medical usage. For example, the particles can be used to kill targets in the human body by hyperthermia (49). This hypothesis arises from a statement of the father of medicine, Hippocrates (460-370 BC), namely: “the diseases which fever cannot cure, those are to be reckoned wholly incurable”. The idea of using magnetic particles for target specific termination is based on the theory that they can generate heat by hysteresis loss under a high frequency magnetic field (49). Another possibility is that the magnetite particles can be used to guide the nanoparticles to a target in the body (50). The nanoparticles are injected close to the target into the bloodstream and a high field/high gradient magnetic field is placed above target site close to the surface of the body. If the location of the target is more interiorly, a magnet can be implanted near the target site to achieve the same goal (51-53).

Multifunctional NPs are one of the main nanomaterials which are currently under investigation, due to their potential utility in a wide arrange of fields. The amount of commercial products which are released on the market and contain NPs is undergoing a rapid increase. Therefore, the possibility of detrimental effects caused by nanoparticle exposure is a growing concern in both the academic and social community. This can be seen in the amount of research that is ongoing in the field of nanotoxicity. Last year in 2012, over 500 articles were published regarding nanoparticle toxicity and almost 16000 citations were made indicating that it is a hot topic (Figure 10).

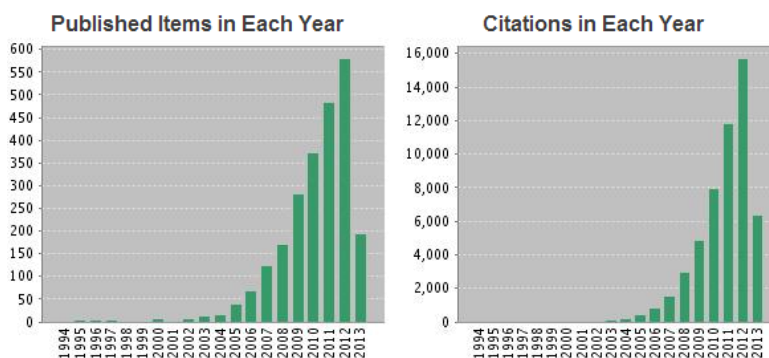


Figure 10. Time table of amount of published articles and citations regarding nanoparticle toxicity (data retrieved from Web of Science).

These nanotoxicology studies investigate the risk associated with inserting nanosystems into the human body, the routes of entry and the molecular mechanisms of occurring toxicity. Despite the ongoing growth in interest in the effects of nanoparticles on the body, a standard procedure to evaluate their effects has not yet been developed. The most desirable tests are those of an *in vivo* nature, since they provide a direct verification of the effects of the nanoparticles on the human body. To this day, however, studies are conducted *in vitro* due to the ease in execution and interpretation and due to human safety laws. *In vitro* studies look at the cytotoxicity on relevant cells that come into contact with the NPs, the cellular uptake of the NPs and the mechanisms behind it, etc. Cytotoxicity can be described as the characteristic of being toxic to cells upon exposure. During this thesis, cell studies are conducted on human microvascular endothelial cell lines (HMEC-1), which are one of the first cells to come into contact with NPs administered intravenously. Both the cytotoxicity and cellular uptake of the discussed NPs is addressed in this work. As a control group, a hybrid model of PLLA NPs encapsulating quantum dots (QDs) was incorporated into the tests. Since PLLA is known for its biocompatibility it can be used as a reference to compare the cytotoxicity of the NPs with. However, since PLLA is not a fluorescent material the QDs were encapsulated in the polymer NPs to serve as a marker. Quantum dots can be defined as very small crystals of semiconducting material with electronic characteristics closely related to their size and shape due to the quantum confinement effect that occurs when the size of the particle is smaller than the exciton Bohr radius. More specifically, the band gap and size are inversely related to each other. By varying the size, one can vary the band gap and therefore the emission wavelength of the particles. Small quantum dots emit high energy light (blue light) while larger quantum dots emit low energy light (red light). The quantum dots used in this thesis had a Cadmium Selenide/Zinc Sulfide (CdSe/ZnS) core-shell composition with a defined fluorescence emission peak at 530 nm. The large difference between the band gap of the CdSe core (1.74 eV) and the ZnS shell (3.61 eV) ensures that the exciton is well confined to the core. The shell also passivates surface defects, which increases the fluorescence quantum yield. (54)

2. Materials & Methods

2.1 Materials

In this section the materials used in the surface functionalization and bioimaging studies are listed.

2.1.1 Surface Functionalization of Polymeric Nanoparticles via Combination of Nitron Chemistry and Miniemulsion Technique

PBN and NHS nitron were synthesized by dra. Kayte Ranieri of the Polymer Reaction Design Group (PRDG) of the Institute for Materials Research (IMO) (20). Cyclohexane (99.5%), sodium dodecyl sulfate (SDS), n-hexadecane (99%) and sodium borohydride (NaBH_4) were obtained from Merck. The 2,2'-Azobis(2-methyl-propionitrile) (AIBN) (98.0%) was bought at Fluka analytical. The DVB (55%), tetrahydrofuran (THF), dimethylformamide (DMF) (99%) and silver nitrate (AgNO_3) (99.9999%) were purchased at Sigma-Aldrich. The aluminum oxide (Al_2O_3) and NIPAAm (99%) were bought at Acros Organics. The Eppendorf vials, denaturated ethanol (95%) and acetone were from VWR. The Amicon ultra filter membrane tubes were purchased at Millipore. The square-mesh copper transmission electron microscopy (TEM) grids were purchased from Electron Microscopy Sciences. The 15 mL centrifuge tubes were bought from Coring Centristar. BupH MES-buffered Saline packs were obtained from Thermo Scientific. The gold labeled goat anti-mouse IgG(H+L) was purchased from KPL. Whatman 150 nm diameter filters were bought at GE healthcare.

2.1.2 Bioimaging using Fluorescent π -conjugated Polymer Nanoparticles

The anionic surfactant SDS was purchased from Merck. MDMO-PPV was synthesized by dra. Neomy Zaquen of the polymer reaction design group of IMO (55). For reference experiments, MDMO-PPV from Sigma-Aldrich was used. Other items purchased at Sigma-Aldrich include PLLA, trypsin, L-glutamine, penicillin/streptomycin (P/S), 98% hydrocortisone (HC), methylthiazolyldiphenyl-tetrazolium bromide (MTT), paraformaldehyde (PFA) and triton X-100. Chloroform (CHCl_3) was bought at AnalaR NORMAPUR. The TEM grids were from Electron Microscopy Science. Magnetite was synthesized by dra. Lien D'Olieslaeger of the materials physics group of IMO (56). The CdSe/ZnS QDs were purchased from PlasmaChem GmbH. The eppendorf vials used for the nanoparticles washing were bought at VWR together with glycine and dimethyl sulfoxide (DMSO). The Amicon ultra filter membrane tubes used for the nanoparticle washing were purchased from Millipore. The T75 culture flask, the 15 mL centrifugation tubes, the 96 flat and v bottom well plates and the 6 well plates were bought at Cellstar. The HMEC-1 cell line was from the Centre of Disease Control and Prevention (Atlanta, GA, USA). The 1x phosphate buffered saline (PBS) solution was purchased at Lonza. Fetal calf serum (FCS), Gibco MCDB 131 medium, recombinant human epidermal growth factor (EGF), 4',6-diamidino-2-phenylindole (DAPI) and Alexa647 phalloidin were bought at Invitrogen. The 0.5% trypan blue in physiological saline was from Biochrom AG. Na-azide was bought at Janssen Chimica. The falcon tubes were from BD Biosciences. The 8 chamber plate and the microscope slides were bought at Thermo Scientific. Fluorescence mounting medium was purchased from Dako. And the nail polish was from Maybelline.

2.2 Methods

In this section the methods used for the surface functionalization and bioimaging studies are summarized.

2.2.1 Surface Functionalization of Polymeric Nanoparticles via Combination of Nitron Chemistry and Miniemulsion Technique

Determination of the partition coefficient of PBN and NHS nitron

Three bottles were weighed before adding concentrations of 20, 40 and 80 mg PBN in 500 mg cyclohexane and 500 mg MilliQ water, to each bottle. The solutions were stirred for 30 min, after which they were left to phase separate. The top phase of each bottle was separated and both phases were evaporated at 40 °C overnight, followed by weighing the bottles. The mass of the bottles was deducted from the mass of the bottles containing the evaporated phases. The percentage of PBN in both phases was determined using the calculated weights and the average was taken of the three concentrations. The same procedure was followed for the NHS nitron, using concentrations of 10 and 15 mg NHS nitron in 500 mg cyclohexane and 500 mg MilliQ water.

“Grafting from” approach using PBN functionality

Synthesis of PBN alkoxyamine functionalities containing polyDVB NPs

First, the continuous phase was prepared by adding 100 mg of SDS to 12 g of MilliQ water. Next, the dispersed phase was prepared by adding 125 mg of HD, 13.4 mg of PBN [75.5 μmol] and 8.9 mg of AIBN [46.29 μmol] to 3 g of over Al_2O_3 percolated DVB [23.04 mmol]. This gives a 1:1 nitron/initiator and 1:500 nitron/DVB molar ratio. The continuous phase was added to the dispersed phase and left to pre-emulsify for 1 h by stirring at room temperature. Then, the mixed solution was ultrasonicated under ice cooling using a Branson 2510 ultrasonicator with a 1/4-tip for 2 min at 65 % using a 30 s pulse and 20 s pause regime. After the ultrasonication step, the mixture was added to a 250 mL round bottom flask and heated to 72 °C for 20 h at a stirring rate of 750 revolutions per minute (rpm). After the reaction the sample was filtered through a paper filter to remove large agglomerates and the solid content was determined thermogravimetrically.

Washing procedure

One milliliter of the sample was transferred to each eppendorf vial and 1 mL of MilliQ water was added. The vials were centrifuged for 3 hours at 14000 rpm with a Sigma 3-30K centrifuge. After centrifugation, the supernatant was removed and the pellet redispersed in 1 mL of MilliQ water. The redispersed solution was moved to membrane tubes in which the sample was washed with MilliQ water by centrifuging 20 times at 2000 rpm for 20 min. After the washing steps, the solid content was determined and transmission electron microscopy (TEM) and dynamic light scattering (DLS) measurements were performed. Afterwards, the sample was freeze-dried. In order to remove any trace of AIBN, if present, the sample was dissolved in THF and centrifuged for 20 min at 14 000 rpm. The supernatant was removed and the pellet redispersed in THF. The redispersed pellet was evaporated overnight at 55 °C. An infrared (IR) spectrum was measured for the sample.

NIPAAm grafting

First, 20 mg of washed NPs was dispersed in 5 mL of DMF and ultrasonicated with a Branson 2510 ultrasonication bath for 3 h on ice. Next, 200 mg of over Al_2O_3 percolated NIPAAm was weighed of in

a 25 mL round bottom flask and the NPs/DMF mixture was added to it. The flask was put on ice and nitrogen flushed for 30 min after which it was put in an oil bath at 110 °C for 4 h at a stirring rate of 1000 rpm. After this period, the sample was washed by centrifuging 4 times in DMF, 3 times in ethanol, 2 times in acetone and 2 times in THF at 9600 rpm for 30 min at 4 °C. As a last washing step, the sample was centrifuged 2 times at 9600 rpm for 40 min at 4 °C in MilliQ water. The sample was characterized with a solid content measurement, ATR-FTIR and TEM.

Silver NPs loading of NIPAAm grafted NPs

The grafted NPs were added to a brown bottle and nitrogen flushed for 30 min at 950 rpm. Then 200 µL of a solution, consisting of 110 µL of a 1:20 in MilliQ water diluted 0.1 M AgNO₃ solution and 90 µL of MilliQ water, was added with a syringe through the septum. The syringe was flushed with another 200 µL of MilliQ water and added to the bottle. Nitrogen flushing was continued for 30 min at 950 rpm. After 30 min, 200 µL of a 1:4.5 diluted 26.4 mM NaBH₄ solution was added with a syringe. The syringe flushing procedure was repeated. The mixture was flushed with nitrogen for 1.5 h at 950 rpm, followed by washing steps. The mixture was transferred to eppendorf vials and centrifuged at 2000 rpm for 20 min, after which the supernatant was transferred to new vials. MilliQ water was added to the supernatant and the vials were centrifuged 2 times for 30 min at 10 000 rpm, replacing the supernatant with MilliQ water and redispersing the pellet. After the last washing step a little bit of MilliQ water was added to the vials to redisperse the pellet and the redispersed solution of each vial was put together and stirred at 200 rpm overnight to completely redisperse the particles. The sample was characterized with TEM and Energy Dispersive X-Ray analysis (EDX).

“Grafting to” approach using NHS nitron functionality

Synthesis and washing NHS nitron alkoxyamine functionalities containing polyDVB NPs

For the synthesis, the same procedure as with PBN was used. In the case of NHS nitron a 1:605 NHS nitron/DVB and 0.8:1 NHS-nitron/initiator molar ratio was taken. This converts in adding 3g [23.04 mmol] DVB, 13.4 mg [41.80 µmol NHS-nitron] and 8.9 mg [46.29 µmol] initiator. After synthesis, 1 mL of sample was transferred to eppendorf vials and supplemented with 1 mL of a mixture consisting of 40 % ethanol and 60 % MilliQ water. The vials were centrifuged at 14000 rpm for 2 h after which the supernatant was removed and the pellet redispersed with the mixture. This was repeated two more times. After the last redispersion step, the redispersed pellet was transferred into membrane tubes and washed 32 times at 2000 rpm for 20 min with MilliQ water. After these washing steps, the solid content was determined and a IR spectrum was made.

Bioconjugation using gold labeled antibody

In order to couple the biomolecules, the washed activated NHS-ester functionalized particles were dispersed in MES buffer (10 mM; pH 7.4) to reach a solid content of 0.5 %. 150 µL gold labeled goat anti-mouse IgG was added and mixed for 3h. After the incubation time, the mixture was centrifuged at 4 °C for 20 min at 2000 rpm to remove larger aggregates. The supernatant was transferred to a new eppendorf vial which was centrifuged at 14000 rpm for 45 min. After this step the supernatant was removed and the pellet redispersed in MilliQ water. Again a centrifugation step was executed of 45 min at 14000 rpm after which the pellet was redispersed. A TEM grid was made of the washed solution.

2.2.2 Bioimaging using Fluorescent π -conjugated Polymer Nanoparticles

Synthesis of MDMO-PPV NPs

First, the continuous phase was made consisting of 72 mg SDS and 24 g MilliQ water. The dispersed phase was built up of 50 mg MDMO-PPV and 1.325 g CHCl_3 . Next, 3.2 g of the continuous phase was added to the dispersed phase, followed by a pre-emulsification step of 1 h stirring at room temperature. The solution was ultrasonicated after pre-emulsification for 3 min (30 s pulse and 20 s pause) at 60 % with a 1/8-tip under ice cooling. The solution was then transferred to a round bottom flask on a hotplate and stirred at 500 rpm for 4 h at 40 °C. After evaporation of chloroform, the sample was filtered. The sample was continuously protected with aluminum foil to prevent degradation. An ultraviolet (UV)-Visible (Vis) spectrum was taken of the MDMO-PPV in CHCl_3 . The solid content was measured thermogravimetrically, the size of the particles was measured using DLS and the morphology of the particles was studied using TEM. Due to the electron beam sensitivity of the material, TEM grids were carbon-coated before putting them in the TEM device.

Synthesis magnetite encapsulated MDMO-PPV NPs, magnetite encapsulated MDMO-PPV/PLLA NPs and QDs encapsulated PLLA NPs

The same protocol as for the MDMO-PPV NPs was used for the synthesis of the other NPs. Only the type and amount of material added differed for every sample (Table 2-1). Also, in case of the magnetite encapsulating samples, a VWR VOS16 mechanical stirrer was used instead of a magnetic stirrer.

Table 2-1. Recipe for synthesis MDMO-PPV/ Fe_3O_4 , MDMO-PPV/PLLA/ Fe_3O_4 and PLLA/QDs NPs

NPs	Continuous Phase	Dispersed Phase
MDMO-PPV/Magnetite	4 g of 72 mg SDS in 24 g MilliQ water	1.6 g CHCl_3
		25 mg Magnetite
		50 mg MDMO-PPV
MDMO-PPV/PLLA/Magnetite	4 g of 72 mg SDS in 24 g MilliQ water	1.6 g CHCl_3
		25 mg Magnetite
		25 mg MDMO-PPV
PLLA/QDs	4 g of 72 mg SDS in 24 g MilliQ water	25 mg PLLA
		1.6 g CHCl_3
		25 mg PLLA
		3 mg QDs

Washing synthesized NPs

The samples were transferred to an eppendorf vial and centrifuged at 2000 rpm for 20 min to remove unencapsulated magnetite or any large aggregates if present. The supernatant was pipetted to a new vial and centrifuged at 14000 rpm for 45 min. After centrifuging the supernatant was removed and the pellet redispersed in MilliQ water. This washing step was done two more times. After the last step the redispersed pellet was transferred to a membrane tube which was centrifuged 20 times at 2000 rpm for 20 min to remove excess surfactant. After each centrifuge step the MilliQ water was replaced and the sample redispersed. When the washing steps were completed, a carbon coated TEM grid was prepared and a solid content measurement was conducted.

Characterization of MDMO-PPV and QDs using UV-Vis spectroscopy

A stock solution of 0.5 mg material in 1 mL of CHCl_3 was made. The following concentrations were made, using this stock solution: 0.3 mg/mL, 0.1 mg/mL, 0.075 mg/mL, 0.025 mg/mL and 0.010 mg/mL. For the MDMO-PPV samples, these concentrations were 1:100 times diluted. The UV-VIS absorbance was measured for the QDs concentrations at $\lambda = 520$ nm, for the polymer reaction design group MDMO-PPV at $\lambda = 508$ nm and for the MDMO-PPV of Sigma-Aldrich at $\lambda = 484$ nm. With these values, the calibration curve was constructed.

HMEC-1 cell culturing procedure

First, the fluid of a T75 flask containing HMEC-1 cells was removed followed by two rinsing steps with 1xPBS. Next, 4 mL of trypsin was added to the flask which was stored for 5 min at 37 °C in a Sanyo CO_2 incubator with a CO_2 level of 5.0 %. After the incubation period, 8 mL of medium solution was added. A 50 mL medium solution consists of 500 μmol L-glutamine, 10 % FCS and 42.5 mL 0.5 % P/S containing MCDB 131 medium. The fluid was resuspended against the wall to detach all the cells from the flask and transferred to a 15 mL centrifuge tube. The tube was centrifuged at 1200 rpm for 8 min with an ALC 4236 centrifuge. After the centrifuge step the tube was emptied and the pellet redispersed in 8 mL of medium solution. From this solution 20 μL was taken and added to an ep which already contained 20 μL of trypan blue. Then, 20 μL of this mixture was taken and added to a Fuchs-Rosenthal counting chamber after which the living cells were counted. To get the total amount of cells in the centrifuge tube the amount of cells in one raster was multiplied with the correction factor 5000, with the dilution factor 2 and with the amount of solution of the centrifuge tube. The known amount of cells was used to make a dilution to get 200 000 cells in the new T75 flask. To this dilution, 20 mL of culture medium was added. An amount of 50 mL culture medium consists of 500 μmol L-glutamine, 10% FCS, 50 μg HC, 500 ng EGF and 42400 μL 0.5% P/S containing MCDB 131 medium. The flask was put into the Sanyo CO_2 incubator with a CO_2 level of 5.0 % at 37 °C for 3 days after which the medium was changed. After 3 more days the cells were split again.

MTT cytotoxicity assay of NPs

HMEC-1 cells were seeded 5000 cells per well on a 96 flat-bottom well plate and the wells were filled up to 100 μL with culture medium. The plates were put into the Sanyo CO_2 incubator at 37 °C with a CO_2 level of 5.0 % for 24 h. After 24 h the solution inside the wells was removed and 100 μL of 1xPBS was added and removed to rinse the wells. Next, 100 μL of the NPs conditions was added in triplicate. The following concentrations were used: 200 $\mu\text{g}/\text{mL}$, 100 $\mu\text{g}/\text{mL}$, 50 $\mu\text{g}/\text{mL}$, 10 $\mu\text{g}/\text{mL}$ and 5 $\mu\text{g}/\text{mL}$. Also 100 μL of a blank and a 100 % cell death condition was added in triplicate. The 100% cell death condition was a 1:9.1 dilution of a 1 g SDS in 10 mL MilliQ. After adding all the conditions, the plates were put into the incubator for another 24 h. After the incubation period, 100 μL of a 1:10 MTT/PBS solution was added to each well after removing the supernatant and the plates were restored into the incubator for an incubation period of 4 h. After 4 h the supernatant was removed and 175 μL of a 1:6 0.1 M Glycine/DMSO solution was added to the wells. After adding the solution, the absorbance was measured at $\lambda = 540$ nm with a FLUOstar OPTIMA and at $\lambda = 570$ nm with a Bio-RAD iMark Microplate Reader.

Fluorescence activated cell sorting NPs uptake study

HMEC-1 cells were seeded out 10 000 cells per well on a 96 flat-bottom well plate and the wells were filled up to 200 μL with culture medium after which the plates were placed in a Sanyo CO_2 incubator at 37 $^\circ\text{C}$ with a CO_2 level of 5 % for 24 h. After the incubation the fluid was removed from the wells and the wells were washed with a 1xPBS solution. Following the rinsing step the conditions were added in quadruplicate. For each sample 100 μL was added of a 1 $\mu\text{g}/\text{mL}$, 5 $\mu\text{g}/\text{mL}$, 10 $\mu\text{g}/\text{mL}$, 50 $\mu\text{g}/\text{mL}$ and 100 $\mu\text{g}/\text{mL}$ solution. Also 4 quadruplicates of only culture medium were made. The plates were put in the incubator for 24 h to take up the NPs. After 24 h, the solution was taken out of the wells and they were rinsed with 1xPBS. Then, 50 μL of trypsin was added and the plates were incubated for 5 min in the incubator after which 50 μL of medium was added. The fluid was resuspended in the wells and transferred to a 96 v-bottom well plate. These plates were then centrifuged for 5 min at 2000 rpm with a Jouan GR422 centrifuge after which the supernatant was removed and 50 μL of fluorescence activated cell sorting (FACS) buffer was added. FACS buffer consists of 1xPBS with 0.1 % Na-Azide and 2 % FCS. The plates were centrifuged at 2000 rpm for 5 min and the supernatant was replaced with 150 μL FACS buffer. After another centrifugation period of 5 min at 2000 rpm the supernatant was removed. The supernatant was replaced with 150 μL of FACS buffer and the plates were centrifuged another time. After this final centrifugation step the supernatant was removed and the pellet resuspended in 150 μL of FACS buffer. This resuspended solution was then transferred to a FACS tube. First gating was performed on the data of the forward versus side scattering plot of a blank of only cells to select the population of cells and filter out debris present. Gating is based on the theory that the scattering depends on the physical properties, which are specific to the type of cell. The forward scattered light is a value proportional to the surface area and size of the cell. The sideward scattered light is proportional to the granularity and internal complexity of the cell. With the gate set the FACS measurement was conducted for each concentration. A 488 nm blue laser was used and the fluorescent signal of the particles was detected in FL2 with band pass filter 585/42. With the data a histogram plot was constructed for each concentration of NPs. The M1 marker was set in this plot to remove any fluorescence caused by the cells themselves. The desired parameters were read from the M2 marker and processed.

Fluorescence microscopy of NPs in fixed HMEC-1 cells

Microscope glasses were placed into a 6 well plate and 20 000 cells were added on top of them together with 100 μL of 200 $\mu\text{g}/\text{mL}$ NPs solution and culture medium to make a total volume of 250 μL . The glasses were then incubated in a Sanyo CO_2 incubator at 37 $^\circ\text{C}$ for 24 h at a CO_2 level of 5 %. After the incubation period the glasses were washed 2 times in 1xPBS for 5 min. The washing was followed by fixing the cells with 4 % PFA for 20 min. Then the glasses were washed 2 more times in 1xPBS for 5 min and incubated in a 0.1 % Triton X solution. The Triton X was removed and the cells were stained with 150 μL of a 0.004 % DAPI/PBS solution for a period of 10 min. The staining was followed by 3 washing steps of 5 min with 1xPBS. A second staining of 20 min with Alexa647 phalloidin was done where 200 μL of a 2.5 % 6.6 μM phalloidin/PBS solution was added to the glasses. The staining was followed by 3 washing steps of 5 min with 1xPBS. After these washing steps, 1 drop of fluorescence mounting medium was put on the glasses, followed by mounting the glasses onto microscope slides. The glass-slide transition was covered with nail polish and the slides were stored in the fridge at 4 $^\circ\text{C}$.

Confocal imaging of NPs in living HMEC-1 cells

HMEC-1 cells were plated out in an 8 chamber plate to which 100 μL of 200 $\mu\text{g}/\text{mL}$ NPs solution and culture medium was added. The plate was incubated for 24 h in a Sanyo CO_2 incubator at 37 $^\circ\text{C}$ with a CO_2 level of 5 %. After the incubation the chambers were rinsed one time with 1xPBS and visualized immediately.

2.2.3 Characterization Methods

Dynamic light scattering

Dynamic light scattering can be used to determine the particle size of synthesized NPs. The technique is based on the Brownian motion of in liquid suspended NPs. By measuring the dynamic fluctuations of the scattered light intensity, one can determine the particle velocity distribution. Using the diffusion coefficient (D), which is inversely proportional to the decay of the light scattering fluctuations, the radius of the NPs can be defined. This feature is done using the Stokes-Einstein equation (Equation 2). (57)

$$R_n = \frac{K_B T}{6 \pi \eta D}$$

Equation 2. Stokes-Einstein equation: K_B , the Boltzman constant; T , temperature of the solvent; η the viscosity.

It should be noted that the radius determined in this manner can be slightly larger than the one observed with a TEM. This is due to the fact that with DLS, the hydrodynamic radius is observed. (57)

During this thesis work, a Brookhaven Instruments Zeta Pals was used for conducting the dynamic light scattering measurements.

Bright field transmission electron microscopy

With transmission electron microscopy one can determine the size and morphology of NPs. The TEM uses an electron gun to shoot electrons in the direction of the sample. These electrons are focused in a beam by electromagnetic lenses, which then travels through the vacuum column to the sample which is located on a copper grid. Depending on the density of the sample, electrons are scattered. These scattered electrons are, unlike the transmitted electrons, not detected in bright field electron microscopy. This leads to a light and shadow effect which is used to define the electron rich regions, which are dark in color, and the electron poor regions, which are light in color. (58)

For this thesis, a TECNAI spirit TEM of FEI was used. The TEM was operated at 120 kV.

Energy-dispersive X-ray spectroscopy

With energy-dispersive X-ray spectroscopy a chemical analysis of NPs can be made. By directing a high-energy beam of electrons at the sample, the inner electrons of the atoms present get excited and are ejected, leaving an electron hole behind. An electron from the outer shell then moves down to fill up the hole. During this process, the energy difference between the inner and outer shell is released in the form of an X-ray. The energy of the emitted X-ray is specific for the atomic structure, which is different for every element. Thus the resulting X-ray spectrum defines which elements are present in the sample. (59)

In this work, energy-dispersive X-ray spectroscopy was conducted with the TECNAI spirit TEM of FEI.

Attenuated total reflectance – Fourier transform infrared spectroscopy

Attenuated total reflectance infrared spectroscopy (ATR) can be used to determine the chemical composition of the NPs. In this technique, a beam of infrared light is directed onto a crystal which is optically dense and has a high refractive index at a particular angle. The resulting internal reflectance leads to the development of an evanescent wave which protrudes 0.5 to 2.0 μm into the sample. When the frequency of the infrared is the same as the vibrational or resonant frequencies of a bond, the sample absorbs energy. This leads to an altered evanescent wave that is detected. From this altered wave, the amount of energy absorbed at each wavelength can be determined with Fourier transformation of the obtained data, providing elemental information of the sample. (60)

In this thesis a Bruker Tensor 27 spectroscope with platinum ATR unit was used.

UV-Vis absorption spectroscopy

UV-Vis absorption spectroscopy is a characterization method which can be used to determine the amount of absorption of electromagnetic radiation, in the visible (400-700 nm) and ultraviolet (200-400 nm) range, by a sample. The radiation is generated with a xenon flash lamp. To measure the absorption at specific wavelengths, the radiation passes through a monochromator before reaching the sample. Electromagnetic rays with a wavelength corresponding to the difference between the ground and excited state of an atom are absorbed and therefore do not pass through the sample.

Two main principles are taken into account when using this technique. The first principle is that the absorption of light is exponentially related to the number of molecules present of the sample, which reflects the concentration. The second principle states that the absorption is exponentially related to the length of the path that the light must travel through the solution. These two principles come together in Beer-Lambert Law (Equation 3). (61)

$$A = \epsilon * l * [C]$$

Equation 3. Beer-Lambert Law: A , absorption; ϵ , constant for solution and wavelength (absorption coefficient); l , length of path traveled by light; C , concentration.

Given that the path length and absorption coefficient are constant during the measurement, there can be concluded from the Beer-Lambert law that a linear relationship between the concentration of sample and the measured absorption is present. Thus, this technique can be used to determine the concentration of absorbing species in a sample. (61)

For this thesis, a Thermo Scientific nanodrop 2000c spectrophotometer was used.

Fluorescence Spectroscopy

Fluorescence spectroscopy is a technique used to detect the emission spectrum of fluorescent substances. The instrument contains three basic items, namely a light source, a sample holder and a detector. The excitation and emission wavelength can be adjusted by the use of monochromatic filters. This setup can be used for measuring the variation in emission intensity with different excitation wavelengths. The resulting spectrum is called the fluorescence emission spectrum. To minimize the photodecomposition of the sample during measurement, the intensity of the incident wavelength is not made to excessive. (62)

The device used for this thesis was a Horiba Jobin Yvon Fluorolog3 Tau.

Fluorescence-activated cell sorting

Fluorescence-activated cell sorting can be used to separate labeled cells from unlabeled cells. In this device, single cells travel in a stream through a laser beam where the fluorescence of each cell is measured. Next, a vibrating nozzle creates droplets which each contain a single cell or nothing. The droplets containing single cells are given a positive or negative charge when they are formed depending on whether or not they contain a fluorescent. The droplets are then separated by a strong electrical field. Clumps of cells which are detected by their increased light scattering are left uncharged and will be discarded into the waste container. These machines can work up to a speed of several thousand cells per second. (63, 64)

The device used for FACS was a Becton Dickinson FACSCalibur.

Confocal Microscopy

As stated previously, an epifluorescence microscope excites all parts of the specimen in the optical path at the same time, which results in an unfocused background part. In confocal microscopy, point illumination is used in combination with a pinhole in an optical conjugate plane in front of the detector to eliminate this out-of-focus signal. The set-up of a confocal microscope is as follows. Coherent light emitted by a laser excitation source travels through a pinhole aperture located in a conjugate plate with a scanning point on the sample. The laser is reflected by a dichromatic mirror and is scanned across the defined focal plane of the sample. The fluorescence emitted from points of the sample travel back through the dichromatic mirror. They are then focused as a confocal point by a second pinhole aperture situated in front of the detector, a photomultiplier tube. Since only the fluorescent light close to the focal plane is detected, the optical resolution of the image is much better. However, longer exposure times are required because most of the fluorescent light is blocked by the pinhole, resulting in a decrease in signal intensity. (65)

A confocal microscope from Carl Zeiss was used.

Epifluorescence Microscopy

In an epifluorescence microscope, light of a certain excitation wavelength is focused on the specimen with an objective lens. The excitation light causes the fluorescent substance in the specimen to emit fluorescence, which is focused by the same objective to the detector. Since most excitation light transmits through the sample, only the emitted light and a small portion of reflected excitation light reaches the detector. To filter out the excitation light, an additional barrier filter is used between the objective and the detector. This results in a high signal to noise ratio. The light sources which are mainly used for this type of microscopy are xenon arc – and mercury-vapor lamps with an excitation filter or high power light emitting diodes. (66)

For this thesis, a NIKON eclipse 80i microscope was used.

3. Results & Discussion

The results of surface functionalization of NPs and bioimaging studies using fluorescent polymer NPs are discussed in the section below.

3.1 Surface Functionalization of Polymeric Nanoparticles *via* Combination of Nitron Chemistry and Miniemulsion Technique

3.1.1 Determination of Partition Coefficients of PBN and NHS Nitron

For heterophase polymerization, it is necessary to determine the solubility of different reactants used in both phases. Therefore, the partition coefficient is determined for the different nitrones. The partition coefficient can be defined as the ratio of the amount of substance in a mixture of two immiscible phases. This value is of importance since it predicts how much of the nitron is present in the hydrophobic dispersed phase and thus participates in the polymerization reaction. Based on this value calculations can be made to balance the molar ratios of the compounds in the synthesis. The average partition coefficients of both the PBN and NHS nitron concentrations determined using cyclohexane and water as two immiscible phases are listed in the table below.

Table 3-1. Partition coefficients PBN and NHS nitron.

Nitron	% in dispersed phase	% in continuous phase
PBN	61.77 %	38.23 %
NHS Nitron	90.90 %	9.10 %

Since direct miniemulsion (oil-in-water) was used, cyclohexane and water are expressed as dispersed and continuous phase respectively. As can be seen 61.77 % of the PBN is found in the dispersed phase compared to 90.90 % in the case of the NHS nitron. This indicates that the NHS nitron is more hydrophobic than PBN. The increase in hydrophobicity can be attributed to the presence of a water-insoluble NHS ester in the structure of the NHS nitron (67).

3.1.2 Synthesis of polyDVB Nanoparticles with ESCP and Miniemulsion Technique

In case of the employment of the miniemulsion technique for the synthesis of NPs built up of DVB, an oil-soluble initiator is used to perform a free radical polymerization reaction in the nanodroplets. In free radical polymerization, a polymer is formed by successive addition of free radical monomer blocks. An example to create free radicals is thermal decomposition, in which the initiator is heated up until a bond in the chemical structure is homolytically cleaved, resulting in two radicals. Other types of initiator decomposition mechanism are photolysis, redox reactions, ionizing radiation, etc. When the free radicals are formed, they add monomer units resulting in the growth of a polymer chain. These polymer chains will crosslink, resulting in the formations of polyDVB NPs. In case of polyDVB synthesized *via* miniemulsion polymerization, a reaction time of 30 min has proven effective for synthesizing particles in the size range ~100 nm (68, 69). As it was the first time that the miniemulsion technique was combined with ESCP, it was therefore necessary to revise the parameters which are normally used for the synthesis of NPs by free radical miniemulsion polymerization.

The first parameter that needed to be defined was the reaction time. When using nitrones in the presence of a monomer and thermal initiator, it is no longer a free radical polymerization reaction but a controlled radical polymerization reaction. This is because the propagating macroradicals are captured by the nitrones, forming alkoxyamines. However, it does not feature living characteristics because the capturing of the radicals is irreversible under normal reaction conditions. The catching of radicals causes a lowering in the number of radicals present in the system, when compared to the uncontrolled polymerization. This leads to a lower rate of polymerization. The reaction time is also influenced by the nitron structure. For this masterthesis a nitron with a N-*t*-butyl substituent was chosen, which leads to a larger steric hindrance resulting in a slower reaction time. However, the reason for choosing this type of nitron is that it shows a better performance in the nitroxide mediated polymerization reaction used later on in the thesis for a 'grafting from' approach. With these properties in mind, the reaction time was increased from 30 min to 20 h. (10, 19)

The second parameter was the choice of initiator that is important to guarantee the presence of mid-chain functionalities. To ensure a maximum formation of mid-chain functionalized DVB polymers, one must carefully look at the attacking initiator radical fragment. The selection process is critical due to competition between the small radical fragments of the initiator and the propagating macroradicals to form either nitroxides or macronitroxide species. In order to minimize the amount of small nitroxides, oxygen-centered radicals need to be avoided while the use of tertiary carbon centered radicals is favored. This is based on the affinity of the radicals for the nitron. Therefore the azoinitiator AIBN was chosen for the polymerization reaction. The optimal amount of the initiator was calculated by taking into account a 1:1 initiator/nitron molar ratio. (19)

Since AIBN is an initiator activated by thermal decomposition, the third parameter investigated was the reaction temperature. The reaction temperature is of importance since it needs to be high enough to decompose the AIBN and low enough to prevent the alkoxyamine bonds from dissociating. AIBN has a working range between 45 and 90 °C, while the decomposition temperature of the alkoxyamine bonds is 80 °C. Therefore a reaction temperature of 72 °C was chosen. (19, 70)

Also the amount of nitron added needed to be determined, since a too large quantity of nitron leads to a too slow reaction rate while a too low quantity of nitron leads to a low grafting density. An optimal result was achieved at a 1:500 nitron/monomer molar ratio.

3.1.3 Grafting From Approach using PBN Functionalities

First the size of the NPs, which had a solid content of 8.1 % before and 2.4 % after washing, was characterized using DLS and TEM. Using DLS a mean size of 134.7 nm was detected with a standard deviation of 5.6 nm and a polydispersity of 0.194. TEM imaging confirmed this size distribution (Figure 11). A mean size of 106.7 nm was measured with a standard deviation of 44.7 nm. The large standard deviation of the TEM image can be attributed to the fact that the mean value was calculated from only the visualized spot, while the DLS measures the mean value for the whole fluid. These values are in good agreement with the literature (71).

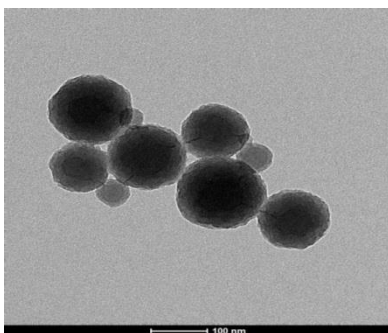


Figure 11. TEM image of polyDVB nanoparticles with PBN nitrono alkoxyamine functionalities.

The next step was to make a composite nanoparticle by using a ‘grafting from’ approach in which a chain of pNIPAAm is synthesized onto the surface. However, this core-shell buildup cannot be visualized by TEM imaging since pNIPAAm is e-beam sensitive and will melt on exposure. Therefore, another characterization method was used. Infrared spectroscopy was chosen to map the chemical structures present in the composite nanoparticles (Figure 12).

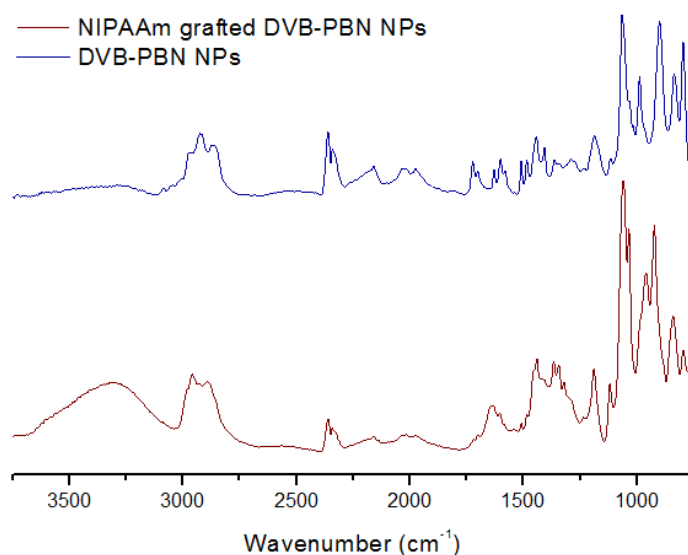


Figure 12. ATR-FTIR spectra of NIPAAm grafted and non-grafted polyDVB nanoparticles.

The infrared spectrum shows a difference in peaks in the region of 1500-1700 cm^{-1} between the grafted and non-grafted sample. In the grafted sample a peak appears at 1657 cm^{-1} . This peak can be attributed to the amide C=O stretch of pNIPAAm, giving strong evidence that the polymer is indeed present on the surface of the nanoparticles (72).

These organic composite nanoparticles were then used to design sophisticated hybrid organic/inorganic nanoparticles by adding an inorganic part. Silver ions were loaded into the pNIPAAm network and by reducing the ions with sodium borohydride, silver NPs were formed within the pNIPAAm shell. The silver ions were located in the pNIPAAm network due to complexation with the nitrogen atoms of NIPAAm (31). To prove the presence of these silver NPs TEM imaging was done in combination with EDX analysis (Figure 13).

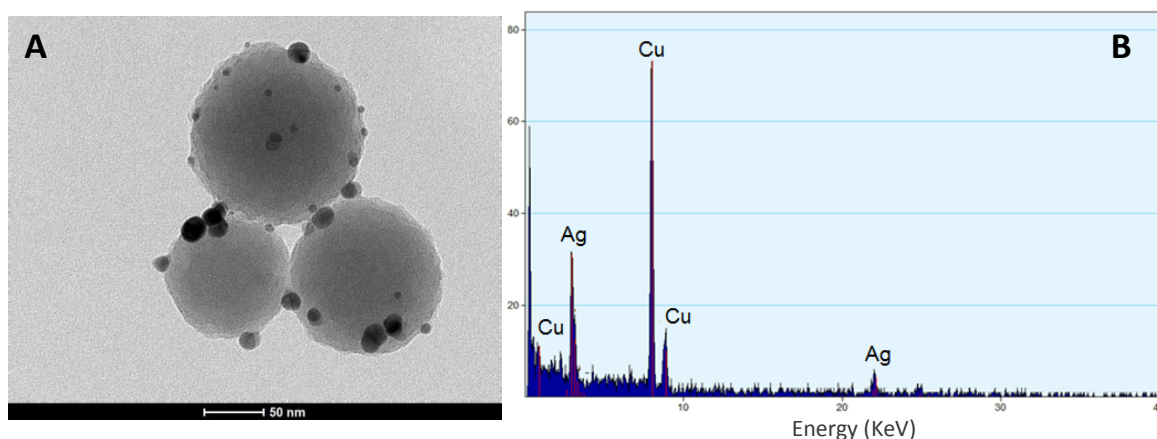


Figure 13. A) TEM image of silver loaded polyDVB-pNIPAAm NPs; B) EDX analysis of silver loaded polyDVB-pNIPAAm NPs.

The TEM image clearly shows the silver nanoparticles surrounding the polyDVB core. Due to their higher electron density more scattering of the electron beam occurs, resulting in darker spots. EDX analysis confirms that these dark spots are indeed silver nanoparticles and not sodium nitrate crystals, a side product of the reduction reaction (73). The characteristic peak belonging to silver nanoparticles can be seen between 2 and 4 KeV (74). The copper peaks are originating from the TEM grids. The TEM image indicates that the silver nanoparticles are indeed truly immobilized in the mesh of the pNIPAAm network, since thorough washing steps were performed. Therefore, the hybrid NPs created with the alkoxyamine functionalities can be considered a stable system. Such a hybrid design was also previously reported for core-shell NPs synthesized using another procedure (31).

3.1.4 Grafting To Approach using NHS Nitron Functionalities

With the solid content of the dispersion being 12.4 % before and 2.3 % after washing, the particle size of the NPs was determined using DLS. A diameter of 75.0 nm was recorded with a standard deviation of 12.5 nm and a polydispersity of 0.298. To prove the presence of the nitron on the surface, an IR spectrum was taken (Figure 14).

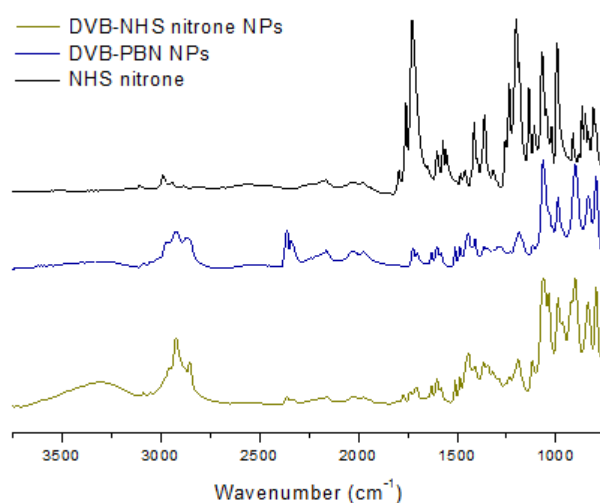


Figure 14. ATR-FTIR spectra of PBN polyDVB nanoparticles, NHS nitron polyDVB nanoparticles and NHS nitron.

New peaks were observed at 1780 cm^{-1} and 1209 cm^{-1} in the spectrum of the NHS nitron polyDVB nanoparticles. The peak at 1780 cm^{-1} correlates to the C=O symmetric stretch of the NHS ester (75). The peak at 1209 cm^{-1} can be attributed to the N-O stretch of the NHS ester (76). Both peaks are found back in the NHS nitron spectrum thus indicating that the NHS nitron is present on the surface of the NPs.

In this case the nitron was used for a 'grafting to' approach. In this approach a pre-synthesized complex is attached to the surface using the functionality. This nitron lends itself to this method due to the presence of the activated NHS ester. Such an activated NHS ester can be used to covalently couple any structure containing a primary amine. When a structure with a primary amine is mixed with a surface containing an activated ester, an amide bond forms, attaching the structure to the surface. In this case gold labeled antibodies were used to couple to the NPs. Antibodies have primary amine groups on the target recognition region in the variable domain of the light chain. Therefore, they can be used for amide bond formation with the NHS nitron containing polyDVB NPs. As a proof of principle, gold labeled antibodies were coupled to the nanoparticle surface and were characterized using TEM (Figure 15).

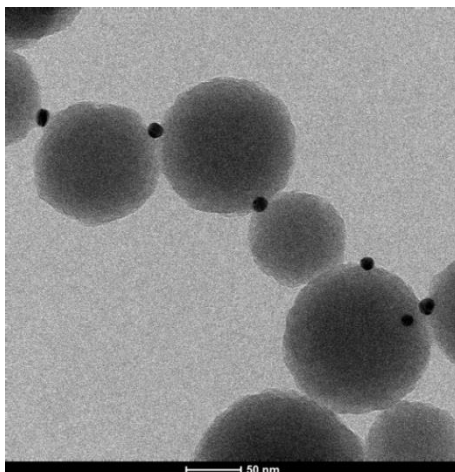


Figure 15. TEM image of gold labeled antibodies attached to NHS nitron polyDVB NPs.

The TEM image clearly demonstrates that the gold labeled antibodies coupled to the NPs. The dark spots on the image represent the gold nanoparticles. Like the silver nanoparticles, these particles have a high electron density resulting in an increase in scattering and therefore a darker tint. This result is in accordance with results previously obtained with an activated NHS on the surface of polyDVB NPs (68). The reason that less gold NPs can be seen when compared with the TEM image of the silver NPs can be attributed to the fact that the amount of NHS ester present on the surface is unknown and that hydrolysis of the existing NHS esters on the surface cannot be excluded. The hydrolysis is correlated to the pH of the reaction solution. NHS esters have a half-life of 4-5 hours at pH 7, 1 h at pH 8 and 10 min at pH 8.6 (77-79). Since the reaction is done at the physiological pH of 7.4 to preserve the biological antibodies, NHS esters on the NPs will be hydrolyzed during the 3 h incubation period resulting in less binding of gold labeled antibodies to the NPs. Also, it is possible that due to the presence of moisture this hydrolysis might have already occurred with the stored NHS nitron.

3.2 Bioimaging using Fluorescent π -conjugated Polymer Nanoparticles

As mentioned before MDMO-PPV is a highly interesting material for bioimaging, but not much is known about its biological effects. Therefore studies were performed to determine the material properties, cell cytotoxicity and cellular uptake, which are discussed in this section. Three buildups were synthesized and studied: Polymer NPs consisting of the semiconducting organic polymer MDMO-PPV, hybrid NPs consisting of organic MDMO-PPV and inorganic magnetite and composite-hybrid Janus NPs comprising of the organic polymers MDMO-PPV and PLLA and inorganic magnetite. As a non-toxic reference for cytotoxicity studies, hybrid NPs were synthesized built up of PLLA and inorganic QDs. The QDs were incorporated to serve as a possible fluorescent marker.

3.2.1 Characterization of the Fluorescent Materials

For nanoparticle-cell interaction studies, the chemical composition of the nanoparticles is very crucial. As we do not have control over the chemical composition of commercially available material, in this work MDMO-PPV synthesized *via* the sulfinyl route by dra. Neomy Zaquen of the PRDG of IMO was used. By using homemade MDMO-PPV the occurrence of cytotoxic effects, caused by unwanted substituents present in a commercial batch which could compromise the cytotoxicity assay, is prevented. It is also worth to note that the sulfinyl route offers materials with superior optical properties. As a reference MDMO-PPV from commercial source (Sigma-Aldrich) was used in this work. The optical properties of both MDMO-PPVs were studied using UV-Vis absorbance and fluorescence spectroscopy measurements to determine if the sulfinyl synthesized MDMO-PPV has comparable characteristics and can thus be used for the synthesis of NPs.

UV-Vis absorbance spectrum

First the absorbance spectrum of both MDMO-PPVs was measured in CHCl_3 using a UV-Vis spectrophotometer (Figure 16). With these spectra, the absorbance maximum peak can be determined for both substances. As can be seen from the spectrum there is a difference in the location of the absorbance maximum. For the commercially available MDMO-PPV the peak is situated at 484 nm, while the peak of the MDMO-PPV obtained from PRDG is located at 508 nm. The difference in the absorbance peak can be attributed to the method of synthesis. An absorbance peak maximum at 508 nm is typical for MDMO-PPV synthesized *via* the sulfinyl precursor route (80). In a precursor route, a substituted and non-conjugated polymer is synthesized, which is then eliminated *via in situ* or post-processing to yield conjugated MDMO-PPV (81). The route of synthesis for the commercial MDMO-PPV is not known, but the absorbance peak correlates with the indicated value of the provider (82). So both are in correlation with the values described in literature.

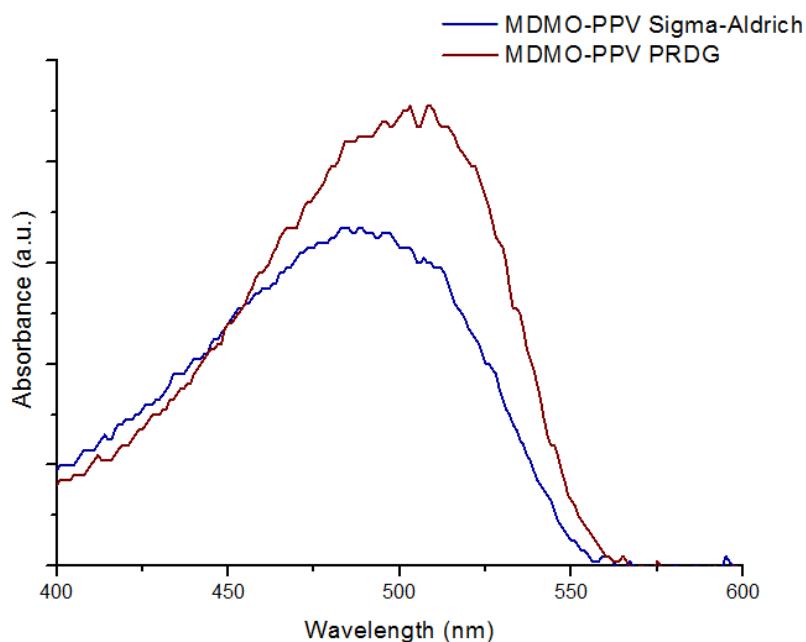


Figure 16. UV-Vis absorbance spectrum of MDMO-PPV from Sigma-Aldrich and PRDG.

Fluorescence emission spectrum

Secondly, the fluorescence emission spectra of the different MDMO-PPVs was determined (Figure 17). The fluorescence emission spectrum was measured by exciting the MDMO-PPV in CHCl_3 with the previously determined absorbance maxima wavelength. Both MDMO-PPV gave an emission peak around 550 nm, which is in accordance with the documented emission value of MDMO-PPV in solution (82, 83).

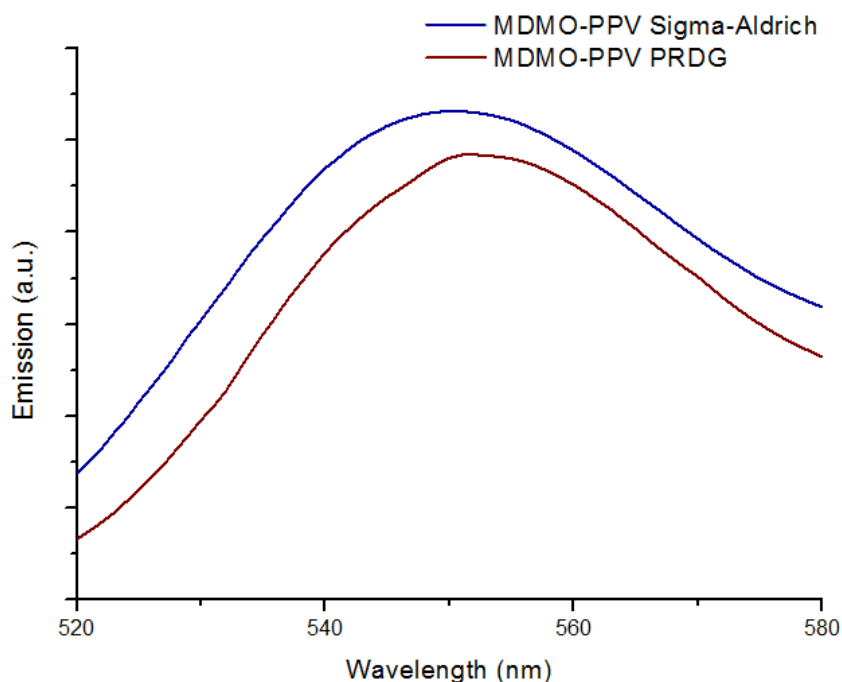


Figure 17. Fluorescence emission spectrum of MDMO-PPV from Sigma-Aldrich and PRDG.

Since these optical studies show that the properties of the homemade MDMO-PPV were equivalent to those of the commercial available MDMO-PPV, the former was employed to synthesize NPs due to its superior purity and tunable characteristics. As previously stated, three buildups were constructed using this material: MDMO-PPV NPs, magnetite encapsulated MDMO-PPV NPs and magnetite encapsulated MDMO-PPV/PLLA NPs. On these buildups cell studies were performed, to determine if a cytotoxic effect was present and to see if the particles were taken up by biologically relevant cells. In order to study the contribution of PLLA, in case of MDMO-PPV/PLLA NPs, in the biocompatibility and cytotoxicity studies, pure PLLA NPs were also made. As PLLA is a non-fluorescent polymer, CdSe/ZnS quantum dots were used as fluorescent markers. These QDs have a known emission wavelength of 530 nm due to their size-band gap relation. However, the absorbance spectrum of this material was not yet known and had to be determined (Appendix Figure A). The absorbance peak for the QDs was located at $\lambda = 520$ nm.

3.2.2 Characterization of the Fluorescent NPs

Once proven that the optical characteristics of the MDMO-PPV obtained from the PRDG were similar to those of commercially available MDMO-PPV, different NPs were synthesized. Before cell experiments were conducted on these NPs, studies were performed to characterize the particles. After synthesis and washing, the size and morphology of these NPs was studied using DLS and TEM and the optical properties were determined using UV-Vis and fluorescence spectroscopy.

Size & morphology characterization of NPs

First the size of the NPs was determined using DLS, of which the results are summarized in table 3-2. Since DLS measures the hydrodynamic radius of the NPs, the measured value is larger than the real value. Therefore, TEM images were used as a second reference. However, the sizes determined by TEM can be correlated to the values measured with DLS for all the samples. Also the solid content of the particles was determined thermogravimetrically before and after washing. The lower solid content after washing can be attributed to the loss of material during the extensive washing steps.

Table 3-2. Overview of solid content, diameter, standard deviation and polydispersity (PDI) values of the different NPs.

NP Model	Solid Content (%)	Solid Content after washing (%)	DLS Diameter (nm)	TEM Diameter (nm)	PDI
MDMO-PPV	1.33	0.15	149.1	120	0.163
MDMO-PPV /Magnetite	1.02	0.09	152.9	112	0.080
MDMO-PPV/PLLA/ Magnetite	1.17	0.11	105.4	75	0.116
PLLA/QDs	2.57	0.67	144.1	100	0.179

The TEM images were not only used as a reference for the size of the particles but also to study their morphology (Figure 18). The first image represents the MDMO-PPV NPs. The dark contrast is caused by the presence of aromatic rings, which makes the molecules electron rich, causing diffraction of the electron beam. The blurred phase around the particles is due to the presence of the surfactant SDS. The presence of this surfactant does however not influence the NP morphology. The second image shows the MDMO-PPV NPs with encapsulated magnetite. The magnetite can be seen as little black dots inside the MDMO-PPV NPs due to its high electron density. The third image represents the MDMO-PPV/PLLA NPs with encapsulated Fe_3O_4 . A clear contrast difference can be noticed between the MDMO-PPV and PLLA. This is because PLLA does not contain aromatic rings and therefore has a lighter contrast in the TEM image. It can be observed that the particles form a Janus-like morphology. In figure 18C inset, a particle showing this morphology is presented. As PLLA is beam sensitive it is difficult to image and also not all the particles are in right orientation to observe Janus morphology. Also, it appears that the magnetite is located solely in the MDMO-PPV part of the NPs. This is a very useful feature since the PLLA part can then be used to encapsulate and release bioactive substances without the risk of releasing magnetite at the same time. The last image (Figure 18D) is a TEM image of the PLLA NPs with encapsulated CdSe/ZnS QDs with the inset depicting encapsulated QDs in an enlarged view. Since PLLA is beam sensitive, the morphology of the particles appears slightly distorted. The inorganic quantum dots appear as dark dots in the TEM image, due to their higher electron density compared to PLLA.

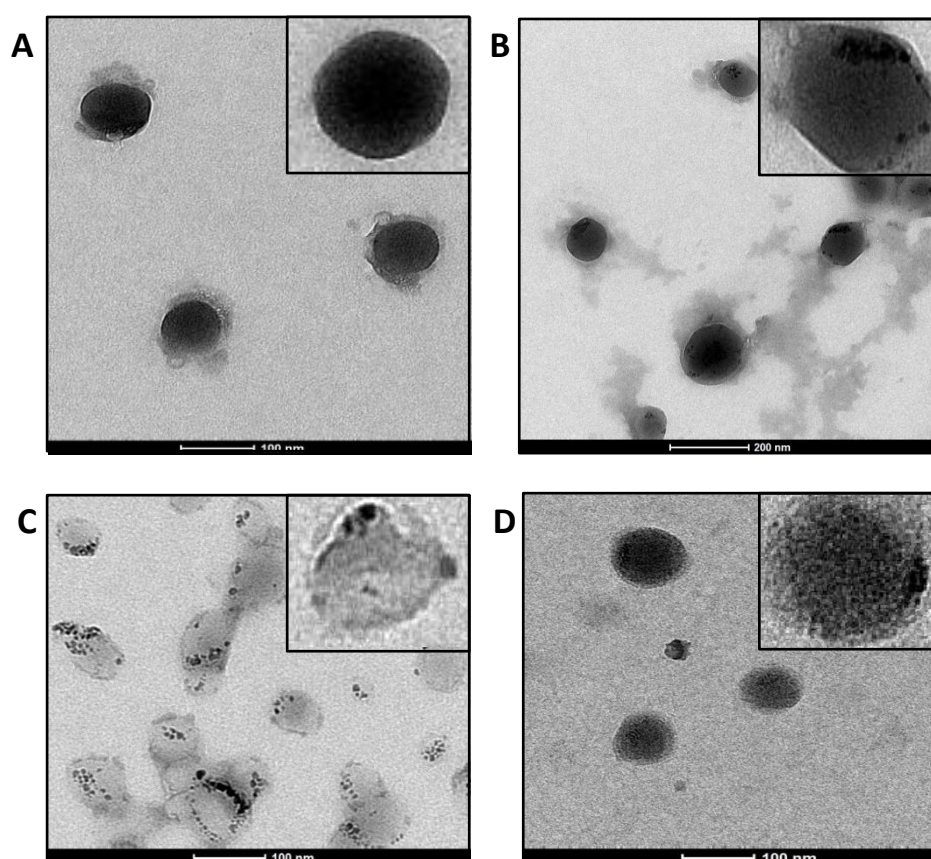


Figure 18. TEM image NP Models. A) MDMO-PPV NPs; B) MDMO-PPV/ Fe_3O_4 NPs; C) MDMO-PPV PRDG/PLLA/ Fe_3O_4 NPs; D) PLLA/QD NPs.

Optical characterization of NPs

Determining the optical properties of the MDMO-PPV NPs is a necessary requirement in order to use them for *in vitro* cell studies. For example, it is essential that the absorbance spectrum of the NPs does not interfere with that of the dyes used to quantify cytotoxicity. Also the excitation and emission wavelengths need to be known to select the proper filters when using FACS, confocal microscopy or epifluorescence microscopy to study the cellular uptake. Eventually, knowledge regarding these characteristics is also required for the long-term goal that is to employ the NPs for bioimaging purposes. The optical properties of the quantum dots were already known and therefore the PLLA/QD model was not included in this study. The optical properties of the other NPs were determined using UV-Vis absorbance and fluorescence spectroscopy.

First, the UV-Vis absorbance spectrum was taken for the 3 buildups of MDMO-PPV NPs dissolved in CHCl_3 (Figure 19). Since the masses of the samples were different, no comparison could be made regarding absorbance intensity. Therefore, to enable a clearer overview of the spectrum progress and the location of the absorbance maximum, the data of the spectra were normalized. The graph with the original spectra can be found in the appendix (Appendix Figure B). The UV-Vis absorbance maximum peaks are located around the same wavelength as that of the MDMO-PPV material from which they were synthesized, namely 508 nm. This was expected as the NPs were synthesized using a solvent/evaporation technique in which NPs are created due to precipitation after evaporation of chloroform. When the NPs are dissolved in chloroform for a UV-Vis absorbance measurement, the polymer is once again molecularly dissolved in the solvent. Also, this proves that ultrasonication does not have a detrimental effect on the optical properties of the material.

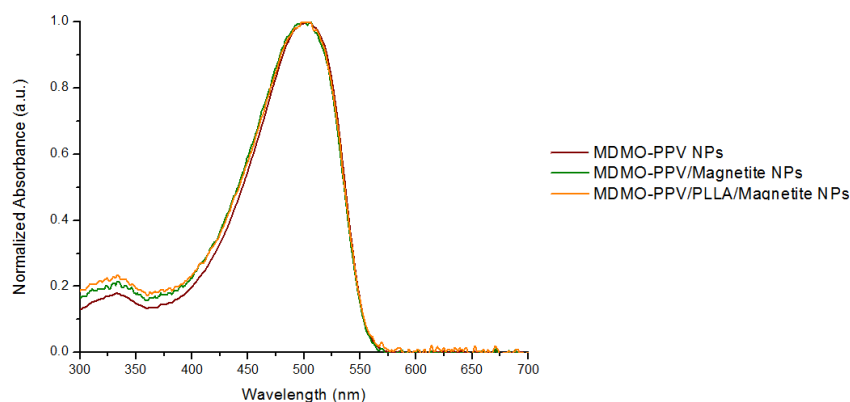


Figure 19. Normalized UV-Vis absorbance spectrum of the NPs.

Not only can the absorbance spectra be used to determine the excitation wavelength for future studies, the non-normalized data can be used to determine the amount of fluorescent material (MDMO-PPV) present in a known amount of sample. By using a calibration curve constructed from the absorbance values of different known concentrations of MDMO-PPV, the amount of fluorescent material could be determined (Appendix Figure C). The determined absorbance maximum value of each sample of NPs, of a known mass, was converted to the concentration of fluorescent material present using the Beer-Lambert law. An overview of the predicted theoretical values, based on the material ratios used during synthesis, and the experimentally determined ones is presented in table 3-3. As can be seen, there is a loss in fluorescent material present. An explanation for this loss can be attributed to the photo- and thermo-oxidation of the polymer. MDMO-PPV can undergo an oxidation process when it is placed in an oxygen containing environment and is exposed to solar light or heat

(84, 85). During this oxidation process, both ether degradation and double-bond saturation occurs. The result of this oxidation process is a loss in intensity of the absorbance peak and a blue shift, indicating the discoloration of the polymer due to a reduction of the conjugation length. A small blue shift occurred in the spectra of all the NP samples, namely from 508 nm to 500 nm. It can be seen that the difference between the theoretical and experimental values of fluorescent material is higher for the magnetite encapsulated NPs. For the magnetite sample, the magnetite to polymer ratio for the synthesized NPs is not known and therefore the encapsulation efficiency could not be determined. The latter can lead to an error in the estimation of solid content (if any unencapsulated magnetite is present) and can contribute to the discrepancy in experimental values as compared to the theoretically determined values. Therefore, a precise thermogravimetric analysis is required to determine the exact ratio of polymer to encapsulated magnetite.

Table 3-3. Concentration of fluorescent material present in sample.

Sample	C_{fluo} (theoretical value)	C_{fluo} (determined value)
	$\mu\text{g}/\text{mg}$ sample	$\mu\text{g}/\text{mg}$ sample
MDMO-PPV NPs	1000	900
MDMO-PPV/Magnetite NPs	667	320
MDMO-PPV/Magnetite/PLLA NPs	333	317

The other optical property that was determined is the fluorescence emission spectrum of the NPs. The spectra were measured by exciting the NPs at their respective absorption maximum wavelength. Again, a graph with normalized data was made to enable a more easy comparison (Figure 20). The normalized emission spectrum of MDMO-PPV was included in the graph to visualize any changes. A shift in the emission maximum peak was noticed from 550 nm to 580 nm. This can be attributed to the difference in measuring a fluorescent raw material sample and a sample of NPs built up from that material. In case of the raw material, only intrachain emission comes into play. When measuring the emission of the fluorescent NPs, interchain emission caused by aggregation of material takes place, which increases the wavelength of the emission maximum and lowers the quantum efficiency. The red shift is due to an increase in overlap of the π -orbitals when the polymer aggregates, which results in the delocalization of the π -electrons across several chains. The delocalization causes the formation of new electronic species with a lower band gap (17, 86). Since the NPs are made *via* a solvent/evaporation technique in which the material precipitates to form NPs, this shift is a logical consequence.

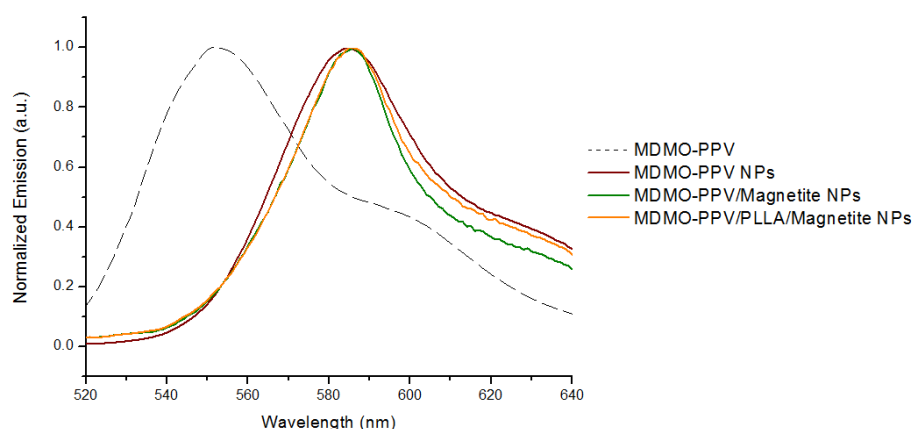


Figure 20. Normalized fluorescence emission spectrum of NPs and MDMO-PPV.

3.2.3 Nanoparticle-cell Interaction Studies

In order to use these NPs for advanced *in vitro* studies and eventually for *in vivo* imaging, it is necessary to know the basic interactions of nanoparticles with cells. In this work, the cytotoxicity and the uptake behavior of NPs was studied. Human microvascular endothelial cells were chosen due to their clinical relevance. They are critical components in wound healing, inflammation, circulation and tumor growth metastases and will be one of the first cells to encounter the particles after injection into the bloodstream. Since MDMO-PPV nanoparticle models are used for the first time to study their cell interaction, literature references are unavailable and firsthand knowledge has to be gained. For the biocompatibility study the MTT assay was used and for the uptake studies fluorescence activated cell sorting (FACS), confocal microscopy and epifluorescence microscopy were employed.

Cytotoxicity studies with HMEC-1 cell lines:

The first test which always precedes every other cellular *in vitro* test is a cytotoxicity assay. It is of great importance to determine whether or not the NPs are cytotoxic for the cells which they will encounter in the human body. If a toxic effect is detected, the particles cannot be used or a new design needs to be considered in which the particles are coated with a biocompatible layer (core-shell buildup). In this thesis a golden standard of the collection of *in vitro* cytotoxicity tests has been used, namely the colorimetric MTT-assay developed in 1983 by T. Mosman. The assay is based upon the reduction of water-soluble, yellow MTT to water-insoluble, purple formazan by viable cells. This insoluble formazan can be detected spectrophotometrically by dissolving it in a DMSO/Glycine solution.

As mentioned previously it is of importance that the absorbance spectrum of the fluorescent material of the NPs does not interfere with that of the cytotoxicity test dye. Otherwise, a higher absorbance value is measured, compromising the test results. To look if interference is present, the absorbance spectrum of in DMSO/Glycine dissolved formazan was compared to that of the NPs determined earlier (Figure 21). Since it was proved already that the absorbance spectra of the different compositions of NPs do not differ, only one buildup was used in the comparison graph. As the solid content varied for both measurements, normalized data was used.

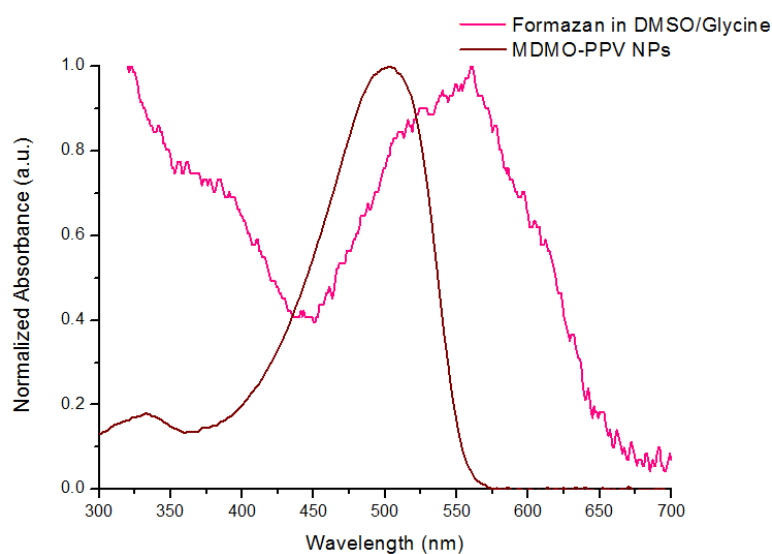


Figure 21. Normalized UV-Vis absorbance spectrum of formazan dissolved in DMSO/Glycine and NPs.

The graph clearly displays some overlap between the two absorption bands. Literature studies have already showed that when the absorption detection wavelength falls in this overlap region, the cell viability measurement is compromised by the interference of the NPs (87, 88). Therefore, the cytotoxicity measurements were performed with a wavelength of 570 nm, which falls out of the absorbance spectrum of the MDMO-PPV NPs. This value lays also outside the narrow absorption peak of the CdSe/ZnS commercial QDs, which has its maximum value at 520 nm and ends at 550 nm.

When adding the DMSO/Glycine solution to the cells, already a colorimetric determination could be made as a preliminary result whether or not the NPs are cytotoxic. Vials which contained living cells colored purple, while vials that contained only death cells remained colorless. The colorimetric result of the MDMO-PPV NPs can be seen in Figure 22, the other ones can be found in the appendix (Appendix Figure D-F). A clear difference in formazan formation was visible between the 100 % cell death and the HMEC-1 cell vials containing different concentrations of NPs. There seemed to be no relation existing between the concentration of NPs and viability of the cells. The blank and NPs wells had the same grade of purple, showing that no or very less cytotoxicity was present. Also, there was no colorimetric difference visible with the eye between the different MDMO-PPV NPs compositions and the biocompatible PLLA/QDs NPs. All these results indicate that the MDMO-PPV particles had probably no direct cytotoxic effect on the HMEC-1 cell line. However it is still possible that there is sublethal damage, which alters certain cell functions. These less obvious toxic effects need to be considered in future research.

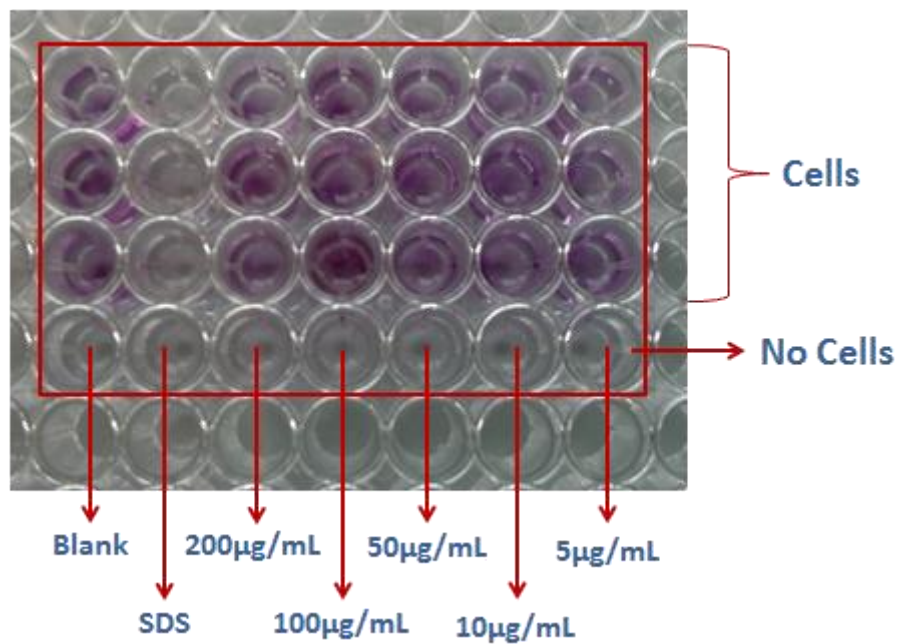


Figure 22. MTT-Assay formazan coloring after 24 h incubation with MDMO-PPV NPs.

However, when trying to measure the absorbance at 570 nm, inconclusive results were obtained (data not shown). Since it was proven that this is not caused by the absorbance of the fluorescent MDMO-PPV, the origin needed to be sought elsewhere. Therefore, the absorbance value at 570 nm for only NPs in medium was measured. High absorbance values were determined for all concentrations of NPs, indicating that the problem is associated with the presence of nanoparticles. Previous literature shows that it is possible for NPs to interfere with an absorbance assay by light scattering (87). Since these NPs were extensively washed to remove all SDS surfactant on the surface, it is possible that they aggregate. This aggregation could increase the intensity of scattering, resulting in a large absorbance value measured. A possible solution to this problem for future studies is to centrifuge the plates and measure only the absorbance of the supernatant. In this way the large aggregates of NPs and cells that could contain these aggregates are removed. Also a control group of only NPs in medium, also centrifuged, can be included to see if there is still scattering present. Also other techniques can be considered to measure the cytotoxicity, for example apoptosis staining with a dye laying outside the emission spectrum of the NPs in combination with epifluorescence microscopy or FACS.

Cellular uptake studies with HMEC-1 cell lines:

Since the preliminary results of the conducted cytotoxicity study indicated that no direct cytotoxic effect was present, first steps towards cellular uptake studies with NPs built up from MDMO-PPV were taken by using FACS, confocal microscopy and epifluorescence microscopy.

The first technique used for the preliminary cellular uptake studies was fluorescence activated cell sorting. FACS was used to determine the number of cells of a population that take up NPs and the mean fluorescent value of the material inside these cells. Different concentrations were used ranging from 1 $\mu\text{g}/\text{mL}$ to 50 $\mu\text{g}/\text{mL}$ of NPs. With the data derived from the M2 marker a cells taking up NPs versus concentration of NPs and a mean fluorescence per cell versus concentration of NPs graph were constructed (Figure 23).

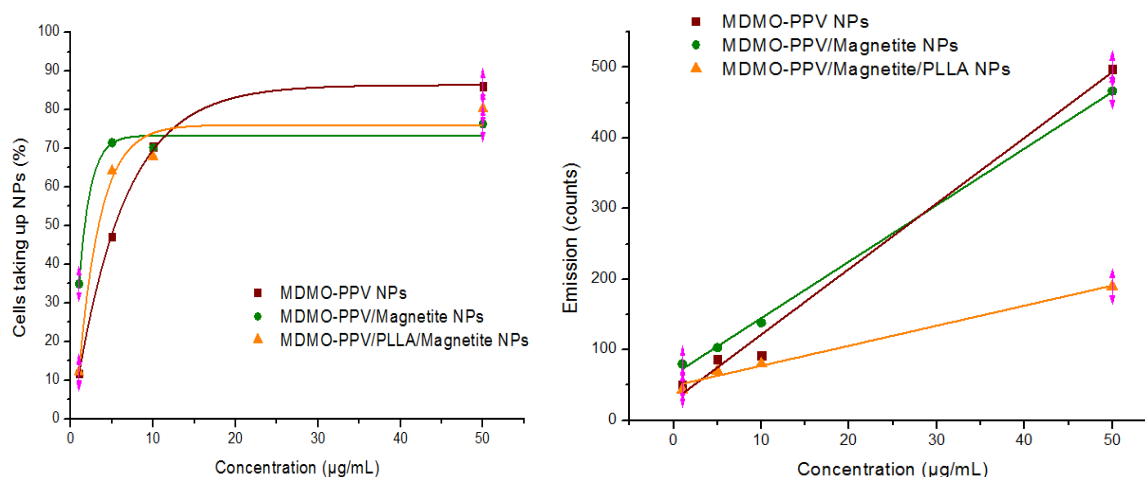


Figure 23. A) Cells taking up NPs versus concentration of different NP models; B) Emission versus concentration of different NP models measured at 585 nm.

The cellular uptake curves were fitted using an exponential function (Figure 23A). This fit resulted in a linearity coefficient of 0.99 for the MDMO-PPV NPs, 0.94 for the MDMO-PPV/Magnetite NPs and 0.93 for the MDMO-PPV/Magnetite/PLLA NPs. All three NP models gave a maximum value of around 80 % with a slight variation between the different models. The graph indicates that already at a concentration of around 20 $\mu\text{g}/\text{mL}$ a maximum number of cells are taking up NPs. There seems to be no sign that increasing the multifunctionality by encapsulating inorganic material or adding another polymer has a large effect on how many cells will take up the NPs.

The mean fluorescence per cell curves were fitted using a linear function (Figure 23B). This fit gave a linearity coefficient of 0.99 for MDMO-PPV NPs, 0.99 for MDMO-PPV/Magnetite NPs and 0.98 for the MDMO-PPV/Magnetite/PLLA NPs. A linear behavior was seen in this figure between the amount of NPs added and the fluorescence. The more MDMO-PPV was added, the higher the mean fluorescence per cell. The reason behind the lower fluorescence of the MDMO-PPV/PLLA Janus particles is that less MDMO-PPV is present in the NPs, 25 mg was used for synthesis compared to 50 mg for the MDMO-PPV and MDMO-PPV/Magnetite particles. Also the small difference between the NPs with and without magnetite can be attributed to the presence of magnetite, which lowers the amount of fluorescent material per gram present. As stated previously further studies need to be conducted to determine the exact amount of magnetite present in the sample.

To not only quantify the amount of cells taking up NPs or the mean fluorescent value per cell but also optically visualize the uptake of the NPs by HMEC-1 cells, confocal and epifluorescence microscopy studies were conducted. First, a confocal microscopy experiment was done to visualize the living HMEC-1 cells after a 24 h incubation period with a known concentration of MDMO-PPV NPs (Figure 24). The MDMO-PPV/Magnetite hybrid NPs and the MDMO-PPV/PLLA/Magnetite composite-hybrid NPs gave a similar result (Appendix Figure H-M). The visualized cells have the typical elongated shape inherent to living endothelial cells. Also, long threadlike extensions called lamellipodia are visible. These are cytoskeletal protein actin extensions which the cell uses to move across the substrate on which it is grown (63). The MDMO-PPV NPs are clearly visible as bright orange dots. Based on the scale bar of 9.46 μm , these dots are in the micrometer range. This indicates that these are not single particles but aggregates. This can be caused by two reasons: either aggregated nanoparticles were taken up by cells (aggregation could be due to excessive washing of surfactant), or the particles were taken up and aggregated in the early or late endosomes of the cells. However, this image does not provide any conclusive proof whether the NPs are located inside or on the membrane of the cells since these measurements were done on living cells that were only rinsed one time with 1xPBS. Also at this point nothing can be stated regarding the uptake mechanisms employed by the HMEC-1 cells to take up the MDMO-PPV NPs.

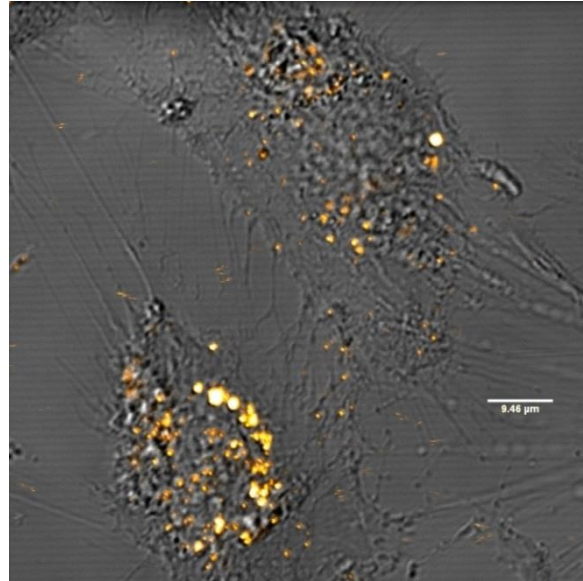


Figure 24. Confocal image of living HMEC-1 cells incubated with MDMO-PPV NPs.

Because the confocal results were inconclusive, another technique was employed to look at the uptake of the NPs by the cells, namely epifluorescence microscopy (Figure 25). This technique gave a better indication of whether the NPs are located outside or on the membrane of the cells, since the HMEC-1 cells were washed extensively with 1xPBS. Also, the F-actine was stained with Alexa Fluor647 phalloidin to visualize the cytoskeleton of the cells and the chromatine was stained with DAPI to visualize the cell nucleus. The picture shows that the nanoparticles are indeed taken up by the cells and are located in the periphery of the nuclear membrane as bright red dots. However, no conclusions can be drawn from these figures to where the NPs are exactly located or how they are taken up. Future experiments are required to determine the uptake mechanisms and which cellular compartments come into play.

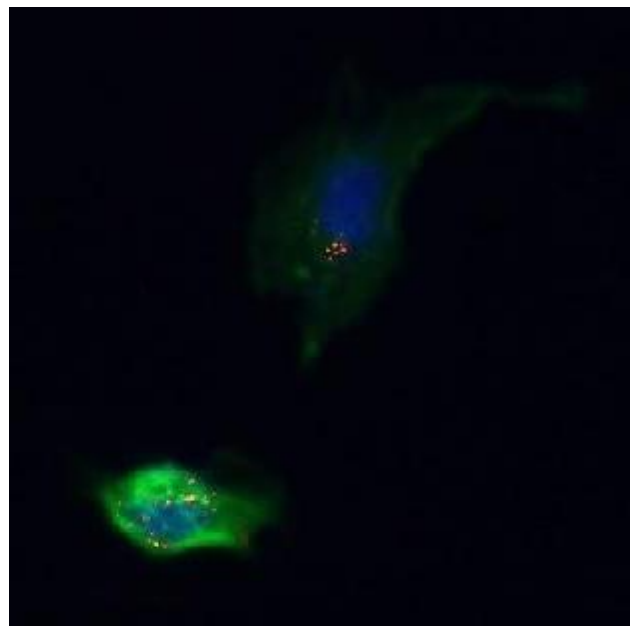


Figure 25. Epifluorescence image of fixed HMEC-1 cells incubated with MDMO-PPV NPs: Blue color is DAPI staining to visualize nucleus, green color is alexa647 phalloidin to visualize the actine and red color is NPs.

4. Conclusion & Outlook

This work deals with the design and development of multifunctional nanoparticles for biomedical applications targeting bioimaging and targeted drug delivery. Multifunctional nanoparticles are superior to monofunctional nanoparticles due to the simple fact that they combine several features, like drug loading, functionalization, imaging, etc. into their design. However, converting these designs from theory to practice is an elaborate multi-step process and still much research is ongoing in search of new materials and methods to simplify this process. During this thesis, two important aspects of multifunctionality were addressed, namely surface functionality (e.g., for (bio-) conjugation) and bioimaging characteristics.

A new method of *in situ* functionalization of nanoparticles was explored in this thesis by combining the miniemulsion technique with enhanced spin capturing polymerization. Through the use of nitrones in the polymerization reaction of the monomer inside the nanodroplet, alkoxyamine functionalities containing polydivinylbenzene nanoparticles in the size range of 100 nm were successfully synthesized. By varying the type of nitron, different functionalities were introduced. Two types of nitron were employed: PBN and NHS nitron. The PBN was used to accomplish a 'grafting from' approach by synthesizing a polyNIPAAm chain onto the particle surface, creating a composite buildup. Since polyNIPAAm is thermoresponsive, this nanoparticle model could provide an interesting new way of thermoresponsive drug delivery when medication is loaded into this polymer shell. However, for this thesis, the model was further extended in a successful manner to a composite-hybrid buildup by incorporating inorganic silver nanoparticles into the polyNIPAAm shell of the particles. Since silver nanoparticles are anti-bacterial, - fungal and -viral, these particles could be used for medical coatings. The second nitron, NHS nitron, was successfully employed in a 'grafting to' approach by using the activated NHS ester on the nitron for bioconjugation. These activated NHS ester containing nanoparticles can be used to couple any biologically relevant molecule which contains an amine group. In this work, as a proof-of-concept, gold labeled IgG antibodies were coupled to the surface of the nanoparticles and were successfully visualized using TEM. This thesis thus proves that the combination of the miniemulsion technique and nitron chemistry provides an easy way of *in situ* functionalization of nanoparticles. Future prospects are to couple relevant biomolecules, like peptides, to the surface using these alkoxyamine functionalities, creating for example targeted nanoparticles. In parallel, (bio-) active ingredients can be encapsulated in these particles, generating a true multifunctional nanoparticle design. Also various nitrones can be tested to introduce new types of functional groups onto the nanoparticle surface.

For the first time, the semiconducting polymer MDMO-PPV, which is well-known for its optoelectronic properties, was introduced in this thesis as a fluorescent marker in the form of nanoparticles for bioimaging. The polymer was synthesized *via* the sulfinyl route by the Polymer Reaction Design Group of the Institute for Materials Research, making it superior to the ones commercially available due to control over the products used. The fluorescent nanoparticles were successfully synthesized using a combination of the solvent/evaporation technique and the miniemulsion technique in which the polymer precipitates into a nanoparticle when evaporating the solvent. Also, the design of the nanoparticles was expanded to a multifunctional one by encapsulating inorganic magnetite (hybrid) or by incorporating a second polymer, namely biodegradable PLLA, together with encapsulated magnetite (composite-hybrid). Magnetite is a

superparamagnetic substance which can be used for targeted guidance of the nanoparticles by applying a magnetic field at the site of interest. PLLA is an FDA approved biodegradable polymer which can be used for loading and releasing of (bio-) active substances. First promising steps were already taken in the direction of *in vivo* imaging by conducting cytotoxicity and cellular uptake studies on HMEC-1 cells in collaboration with the Immunology group of BIOMED, generating protocols for future studies since it was the first time that these type of nanoparticles were tested on cells. The HMEC-1 cells were chosen due to the fact that they are part of the blood vessels and thus are exposed early to NPs when these are injected into the human body. Preliminary results show that these particles are taken up by the endothelial cells and are not cytotoxic. The MDMO-PPV nanoparticles have a great future ahead due to their superiority compared to small dye molecules and quantum dots. In the short term, experiments need to be done to quantify the cytotoxicity of the nanoparticles and to look at the magnetite/sample ratio of the nanoparticles. In the long term, the knowledge concerning the cell-nanoparticle interactions needs to be expanded by carefully planning out further studies to underpin the effects of the material composition, size and surface charge.

References

1. Feynman RP. The pleasure of finding things out: The best short works of Richard P. Feynman: Basic Books; 2005.
2. TC P, Mathew L, Chandrasekaran N, Raichur AM, Mukherjee A. Biomimetic Synthesis of Nanoparticles: Science, Technology & Applicability.
3. Sanvicens N, Marco MP. Multifunctional nanoparticles--properties and prospects for their use in human medicine. *Trends in Biotechnology*. 2008; 26(8): 425-33.
4. Sperling R, Parak W. Surface modification, functionalization and bioconjugation of colloidal inorganic nanoparticles. *Philosophical Transactions of the Royal Society A: Mathematical, Physical and Engineering Sciences*. 2010; 368(1915): 1333-83.
5. Soenen SJ, Rivera-Gil P, Montenegro J-M, Parak WJ, De Smedt SC, Braeckmans K. Cellular toxicity of inorganic nanoparticles: Common aspects and guidelines for improved nanotoxicity evaluation. *Nano Today*. 2011; 6(5): 446-65.
6. Alkilany AM, Murphy CJ. Toxicity and cellular uptake of gold nanoparticles: what we have learned so far? *Journal of nanoparticle research : an interdisciplinary forum for nanoscale science and technology*. 2010; 12(7): 2313-33.
7. Nahar M, Dutta T, Murugesan S, Asthana A, Mishra D, Rajkumar V, et al. Functional polymeric nanoparticles: an efficient and promising tool for active delivery of bioactives. *Critical Reviews in Therapeutic Drug Carrier Systems*. 2006; 23(4): 259-318.
8. Puri S. Novel Functionalized Polymers for Nanoparticle Formulations with Anti Cancer Drugs. PhD Thesis University of Nottingham. 2007.
9. Patil YB, Toti US, Khair A, Ma L, Panyam J. Single-step surface functionalization of polymeric nanoparticles for targeted drug delivery. *Biomaterials*. 2009; 30(5): 859-66.
10. Barner L, Quick AS, Vogt AP, Winkler V, Junkers T, Barner-Kowollik C. Thermally responsive core-shell microparticles and cross-linked networks based on nitrene chemistry. *Polymer Chemistry*. 2012; 3(8): 2266-76.
11. Riehemann K, Schneider SW, Luger TA, Godin B, Ferrari M, Fuchs H. Nanomedicine--challenge and perspectives. *Angewandte Chemie*. 2009; 48(5): 872-97.
12. Weiss KC, Lorenz RM, Landfester K, Mailänder V. Cellular Uptake Behavior of Unfunctionalized and Functionalized PBCA Particles Prepared in a Miniemulsion *Macromolecular Bioscience*. 2007; 7: 883-96.
13. D'Olieslaeger L. Multifunctional Hybrid Nanoparticles for Biomedical Applications UHasselt; 2012.
14. Bera D, Qian L, Tseng T-K, Holloway PH. Quantum Dots and Their Multimodal Applications: A Review. *Materials*. 2010; 3(4): 2260-345.
15. Facchetti A. π -Conjugated Polymers for Organic Electronics and Photovoltaic Cell Applications†. *Chemistry of Materials*. 2010; 23(3): 733-58.
16. Jarzab D, Lu M, Nicolai HT, Blom PWM, Loi MA. Photoluminescence of conjugated polymer blends at the nanoscale. *Soft Matter*. 2011; 7(5): 1702-7.
17. Green M, Howes P, Berry C, Argyros O, Thanou M. Simple conjugated polymer nanoparticles as biological labels. *Proceedings of the Royal Society A: Mathematical, Physical and Engineering Science*. 2009; 465(2109): 2751-9.
18. Tuncel D, Demir HV. Conjugated polymer nanoparticles. *Nanoscale*. 2010; 2(4): 484-94.
19. Wong EHH, Junkers T, Barner-Kowollik C. Nitrenes in synthetic polymer chemistry. *Polymer Chemistry*. 2011; 2(5): 1008-17.
20. Zang L, Wong EHH, Barner-Kowollik C, Junkers T. Control of methyl methacrylate radical polymerization via Enhanced Spin Capturing Polymerization (ESCP). *Polymer*. 2010; 51(17): 3821-5.

21. Costello PA, Martin IK, Slark AT, Sherrington DC, Titterton A. Branched methacrylate copolymers from multifunctional monomers: chemical composition and physical architecture distributions. *Polymer*. 2002; 43(2): 245-54.
22. Goldmann AS, Walther A, Nebhani L, Joso R, Ernst D, Loos K, et al. Surface Modification of Poly(divinylbenzene) Microspheres via Thiol–Ene Chemistry and Alkyne–Azide Click Reactions. *Macromolecules*. 2009; 42(11): 3707-14.
23. Cormack PAG, Davies A, Fontanals N. Synthesis and characterization of microporous polymer microspheres with strong cation-exchange character. *Reactive and Functional Polymers*. 2012; 72(12): 939-46.
24. Durmaz YY, Karagoz B, Bicak N, Demirkol DO, Yalcinkaya EE, Timur S, et al. Modification of polydivinylbenzene microspheres by a hydrobromination/click-chemistry protocol and their protein-adsorption properties. *Macromolecular Bioscience*. 2011; 11(1): 141-50.
25. Mittal V. *Miniemulsion Polymerization Technology*: Wiley; 2011.
26. Schubert S, Delaney JJT, Schubert US. Nanoprecipitation and nanoformulation of polymers: from history to powerful possibilities beyond poly(lactic acid). *Soft Matter*. 2011; 7(5): 1581-8.
27. Kotti K, Kiparissides C. Synthesis of Composite Polystyrene/Silica Nanoparticles via Precipitation and Emulsion Polymerization Methods. *Macromolecular Reaction Engineering*. 2010; 4(5): 347-57.
28. Elbert DL. Liquid-liquid two-phase systems for the production of porous hydrogels and hydrogel microspheres for biomedical applications: A tutorial review. *Acta Biomaterialia*. 2011; 7(1): 31-56.
29. Ethirajan A, Landfester K. Functional hybrid materials with polymer nanoparticles as templates. *Chemistry*. 2010; 16(31): 9398-412.
30. Landfester K. Polyreactions in Miniemulsions. *Macromolecular Rapid Communications*. 2001; 22(12): 896-936.
31. Lu Y, Mei Y, Drechsler M, Ballauff M. Thermosensitive core-shell particles as carriers for ag nanoparticles: modulating the catalytic activity by a phase transition in networks. *Angewandte Chemie*. 2006; 45(5): 813-6.
32. Lara HH, Garza-Trevino EN, Ixtepan-Turrent L, Singh DK. Silver nanoparticles are broad-spectrum bactericidal and virucidal compounds. *Journal of Nanobiotechnology*. 2011; 9: 30.
33. Lara HH, Ayala-Nunez NV, Ixtepan-Turrent L, Rodriguez-Padilla C. Mode of antiviral action of silver nanoparticles against HIV-1. *Journal of Nanobiotechnology*. 2010; 8: 1.
34. Panacek A, Kolar M, Vecerova R, Prucek R, Soukupova J, Krystof V, et al. Antifungal activity of silver nanoparticles against *Candida* spp. *Biomaterials*. 2009; 30(31): 6333-40.
35. de Mol NJ, Fischer MJ. Surface plasmon resonance: a general introduction. *Methods in Molecular Biology*. 2010; 627: 1-14.
36. Thomas III S, Swager T. *Conjugated Polymer Sensors: Design Principles Towards Enhanced Versatility*. DTIC Document, 2004.
37. Brabec C, Cravino A, Zerza G, Sariciftci N, Kiebooms R, Vanderzande D, et al. Photoactive Blends of Poly (p ara-phenylenevinylene)(PPV) with Methanofullerenes from a Novel Precursor: Photophysics and Device Performance. *The Journal of Physical Chemistry B*. 2001; 105(8): 1528-36.
38. Peeters M, Troost FJ, van Grinsven B, Horemans F, Alenus J, Murib MS, et al. MIP-based biomimetic sensor for the electronic detection of serotonin in human blood plasma. *Sensors and Actuators B: Chemical*. 2012; 171–172(0): 602-10.
39. Vandenberg J, Cosmans I, Lutsen L, Vanderzande D, Junkers T. Controlled synthesis of MDMO-PPV and block copolymers made thereof. *Polymer Chemistry*. 2012; 3(7): 1722-5.
40. Ethirajan A, Musyanovych A, Chuvilin A, Landfester K. Biodegradable Polymeric Nanoparticles as Templates for Biomimetic Mineralization of Calcium Phosphate. *Macromolecular Chemistry and Physics*. 2011; 212(9): 915-25.

41. Landfester K. Miniemulsion polymerization and the structure of polymer and hybrid nanoparticles. *Angewandte Chemie*. 2009; 48(25): 4488-507.
42. Cooreman P, Thoelen R, Manca J, vandeVen M, Vermeeren V, Michiels L, et al. Impedimetric immunosensors based on the conjugated polymer PPV. *Biosensors and Bioelectronics*. 2005; 20(10): 2151-6.
43. Ghazy O. Binary Blend Nanoparticles with Defined Morphology; 2008.
44. Chen YC, Dimonie V, El-Aasser MS. Effect of interfacial phenomena on the development of particle morphology in a polymer latex system. *Macromolecules*. 1991; 24(13): 3779-87.
45. Jiang S, Chen Q, Tripathy M, Luijten E, Schweizer KS, Granick S. Janus particle synthesis and assembly. *Advanced materials*. 2010; 22(10): 1060-71.
46. Xu H, Deshmukh R, Timmons R, Nguyen KT. Enhanced endothelialization on surface modified poly(L-lactic acid) substrates. *Tissue Engineering Part A*. 2011; 17(5-6): 865-76.
47. Zeronian SH, Collins MJ. Surface modification of polyester by alkaline treatments. *Textile Progress*. 1989; 20(2): 1-26.
48. Jeong U, Teng X, Wang Y, Yang H, Xia Y. Superparamagnetic Colloids: Controlled Synthesis and Niche Applications. *Advanced Materials*. 2007; 19(1): 33-60.
49. Pankhurst QA, Connolly J, Jones SK, Dobson J. Applications of magnetic nanoparticles in biomedicine. *Journal of Physics D: Applied Physics*. 2003; 36(13): R167.
50. McBain SC, Yiu HH, Dobson J. Magnetic nanoparticles for gene and drug delivery. *International Journal of Nanomedicine*. 2008; 3(2): 169-80.
51. Fernández-Pacheco R, Valdivia JG, Ibarra MR. Magnetic Nanoparticles for Local Drug Delivery Using Magnetic Implants. In: Foote RS, Lee JW, editors. *Micro and Nano Technologies in Bioanalysis. Methods in Molecular Biology™*. 544: Humana Press; 2009. p. 559-69.
52. Yellen BB, Forbes ZG, Halverson DS, Fridman G, Barbee KA, Chorny M, et al. Targeted drug delivery to magnetic implants for therapeutic applications. *Journal of Magnetism and Magnetic Materials*. 2005; 293(1): 647-54.
53. Rosengart AJ, Kaminski MD, Chen H, Caviness PL, Ebner AD, Ritter JA. Magnetizable implants and functionalized magnetic carriers: A novel approach for noninvasive yet targeted drug delivery. *Journal of Magnetism and Magnetic Materials*. 2005; 293(1): 633-8.
54. Angell JJ. Synthesis and Characterization of CdSe-ZnS Core-Shell Quantum Dots for Increased Quantum Yield. 2011.
55. van Breemen AJJM, Vanderzande DJM, Adriaensens PJ, Gelan JMJV. Highly Selective Route for Producing Unsymmetrically Substituted Monomers toward Synthesis of Conjugated Polymers Derived from Poly(p-phenylene vinylene). *The Journal of Organic Chemistry*. 1999; 64(9): 3106-12.
56. Urban M, Musyanovych A, Landfester K. Fluorescent Superparamagnetic Polylactide Nanoparticles by Combination of Miniemulsion and Emulsion/Solvent Evaporation Techniques. *Macromolecular Chemistry and Physics*. 2009; 210(11): 961-70.
57. Berne BJ, Pecora R. *Dynamic Light Scattering: With Applications to Chemistry, Biology and Physics*: DOVER PUBN Incorporated; 2000.
58. Reimer L, Kohl H. *Transmission Electron Microscopy: Physics of Image Formation and Microanalysis*: Springer; 2008.
59. Goldstein J. *Scanning electron microscopy and x-ray microanalysis*: Kluwer Academic/Plenum Publishers; 2003.
60. Griffiths PR, de Haseth JA. *Attenuated Total Reflection. Fourier Transform Infrared Spectrometry*: John Wiley & Sons, Inc.; 2006. p. 321-48.
61. Upstone SL. *Ultraviolet/Visible Light Absorption Spectrophotometry in Clinical Chemistry*. In: Meyers RA, editor. *Encyclopedia of Analytical Chemistry*. Chichester: John Wiley & Sons Ltd; 2000.
62. *An Introduction to Fluorescence Spectroscopy* PerkinElmer Ltd; 2000.
63. Boyle J. *Molecular biology of the cell*, 5th edition by B. Alberts, A. Johnson, J. Lewis, M. Raff, K. Roberts, and P. Walter. *Biochemistry and Molecular Biology Education*. 2008; 36(4): 317-8.

64. Shapiro HM. Practical Flow Cytometry: Wiley; 2005.
65. Combs CA. Fluorescence microscopy: A concise guide to current imaging methods. Current Protocols in Neuroscience. 2010; 2.1. -2.1. 14.
66. Petty HR. Fluorescence microscopy: Established and emerging methods, experimental strategies, and applications in immunology. Microscopy Research and Technique. 2007; 70(8): 687-709.
67. G-Biosciences. Protein Cross-Linkers: Handbook & Selection Guide.
68. Ethirajan A, Baeten L, Conradi M, Ranieri K, Conings B, Boyen H-G, et al. UV-induced functionalization of poly(divinylbenzene) nanoparticles via efficient [2 + 2]-photocycloadditions. Polymer Chemistry. 2013.
69. Choi EC, Jin SM, Park YJ, Kim Y. Polymerization kinetics for the preparation of poly(*p*-divinylbenzene) via a miniemulsion polymerization process. Journal of the Chinese Institute of Chemical Engineers. 2008; 39(5): 483-8.
70. <http://www.biolar.lv/web/en/22-azobisisobutyronitrile-aibn.html>: biolar; [01/06/2013].
71. Bach T. Stereoselective intermolecular [2+2]-photocycloaddition reactions and their application in synthesis. Synthesis. 2000; 1998(05): 683-703.
72. Zhang J, Peppas NA. Molecular interactions in poly (methacrylic acid)/poly (N-isopropyl acrylamide) interpenetrating polymer networks. Journal of applied polymer science. 2001; 82(5): 1077-82.
73. Mulfinger L, Solomon SD, Bahadory M, Jeyarajasingam AV, Rutkowsky SA, Boritz C. Synthesis and study of silver nanoparticles. Journal of Chemical Education. 2007; 84(2): 322.
74. Puchalski M, Dąbrowski P, Olejniczak W, Krukowski P, Kowalczyk P, Polański K. The study of silver nanoparticles by scanning electron microscopy, energy dispersive X-ray analysis and scanning tunnelling microscopy. Materials Science-Poland. 2007; 25(2): 473-8.
75. Wang C, Yan Q, Liu H-B, Zhou X-H, Xiao S-J. Different EDC/NHS activation mechanisms between PAA and PMAA brushes and the following amidation reactions. Langmuir. 2011; 27(19): 12058-68.
76. Lee JY, Lee J-W, Schmidt CE. Neuroactive conducting scaffolds: nerve growth factor conjugation on active ester-functionalized polypyrrole. Journal of the Royal Society Interface. 2009; 6(38): 801-10.
77. Lomant AJ, Fairbanks G. Chemical probes of extended biological structures: Synthesis and properties of the cleavable protein cross-linking reagent [³⁵S] dithiobis (succinimidyl propionate). Journal of Molecular Biology. 1976; 104(1): 243-61.
78. Staros JV, Wright RW, Swingle DM. Enhancement by *N*-hydroxysulfosuccinimide of water-soluble carbodiimide-mediated coupling reactions. Analytical Biochemistry. 1986; 156(1): 220-2.
79. Cuatrecasas P, Parikh I. Adsorbents for affinity chromatography. Use of *N*-hydroxysuccinimide esters of agarose. Biochemistry. 1972; 11(12): 2291-9.
80. Van Severen I, Breselge M, Fourier S, Adriaensens P, Manca J, Lutsen L, et al. 2,5-Substituted PPV-Derivatives with Different Polarities: The Effect of Side Chain Polarity on Solubility, Optical and Electronic Properties. Macromolecular Chemistry and Physics. 2007; 208(2): 196-206.
81. Cosemans I, Wouters J, Cleij T, Lutsen L, Maes W, Junkers T, et al. Living Polymerization via Anionic Initiation for the Synthesis of Well-Defined PPV Materials. Macromolecular Rapid Communications. 2012; 33(3): 242-7.
82. Sigma-Aldrich.
<http://www.sigmaaldrich.com/catalog/product/aldrich/546461?lang=en®ion=BE>
[02/06/2013].
83. Lockwood DJ, Mascher P. Nanoscale Luminescent Materials: Electrochemical Society; 2010.

84. Chambon S, Rivaton A, Gardette J-L, Firon M, Lutsen L. Aging of a donor conjugated polymer: Photochemical studies of the degradation of poly[2-methoxy-5-(3',7'-dimethyloctyloxy)-1,4-phenylenevinylene]. *Journal of Polymer Science Part A: Polymer Chemistry*. 2007; 45(2): 317-31.
85. Krebs FC. *Stability and Degradation of Organic and Polymer Solar Cells*: Wiley; 2012.
86. Psiachos D, Mazumdar S. Correlated-electron description of the photophysics of thin films of π -conjugated polymers. *Physical Review B*. 2009; 79(15): 155106.
87. Kong B, Seog JH, Graham LM, Lee SB. Experimental considerations on the cytotoxicity of nanoparticles. *Nanomedicine*. 2011; 6(5): 929-41.
88. Dobrovolskaia MA, Clogston JD, Neun BW, Hall JB, Patri AK, McNeil SE. Method for analysis of nanoparticle hemolytic properties in vitro. *Nano Letters*. 2008; 8(8): 2180-7.

Appendix

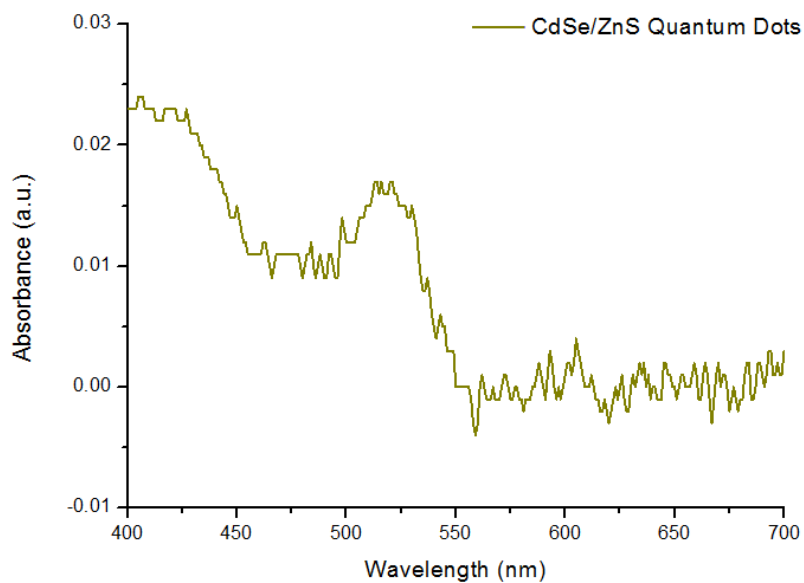


Figure A. UV-Vis absorbance spectrum of CdSe/ZnS quantum dots.

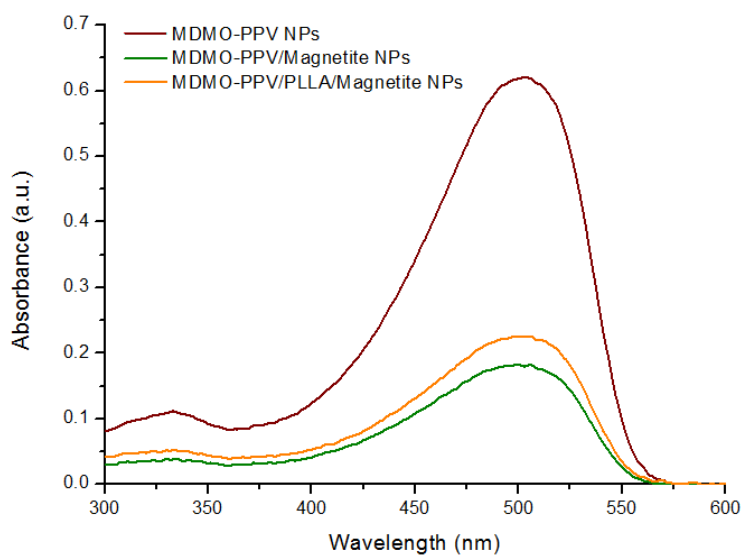


Figure B. UV-Vis absorbance spectrum of the NPs.

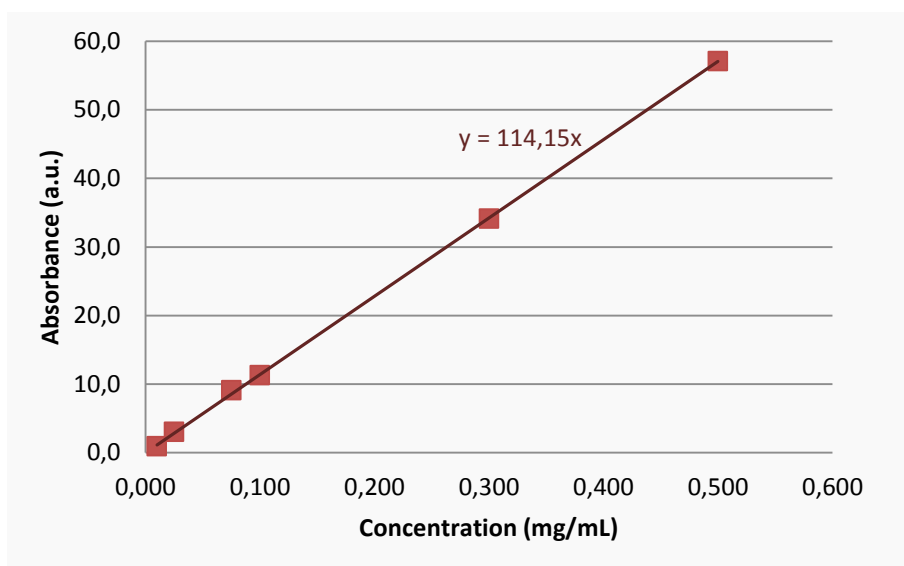


Figure C. Calibration curve MDMO-PPV PRDG.

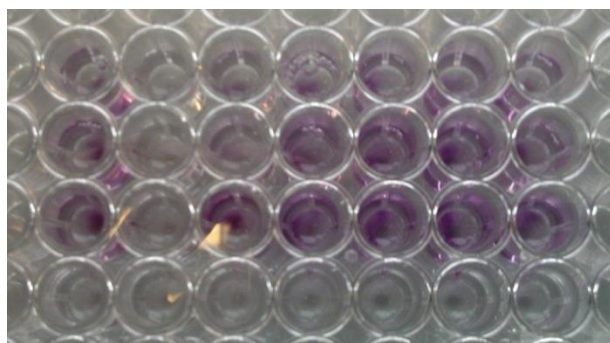


Figure D. Colorimetric result MDMO-PPV/Magnetite NPs.

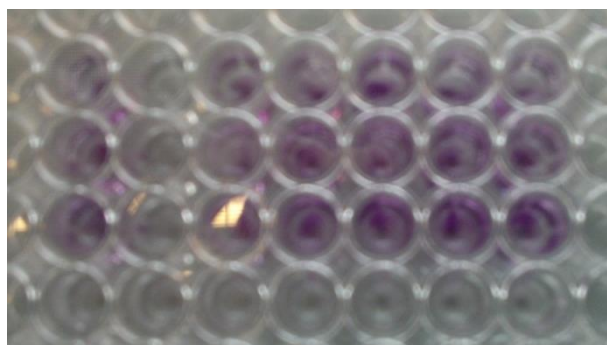


Figure E. Colorimetric result MDMO-PPV/PLLA/Magnetite NPs.

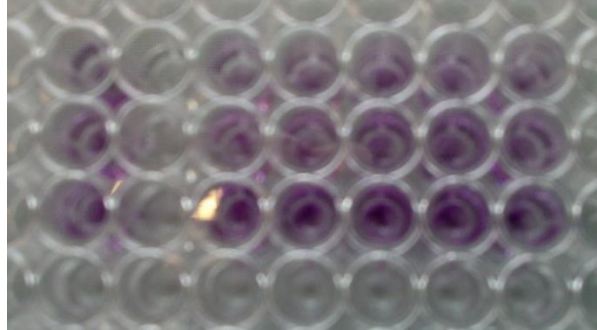


Figure F. Colorimetric result PLLA/QDs NPs.

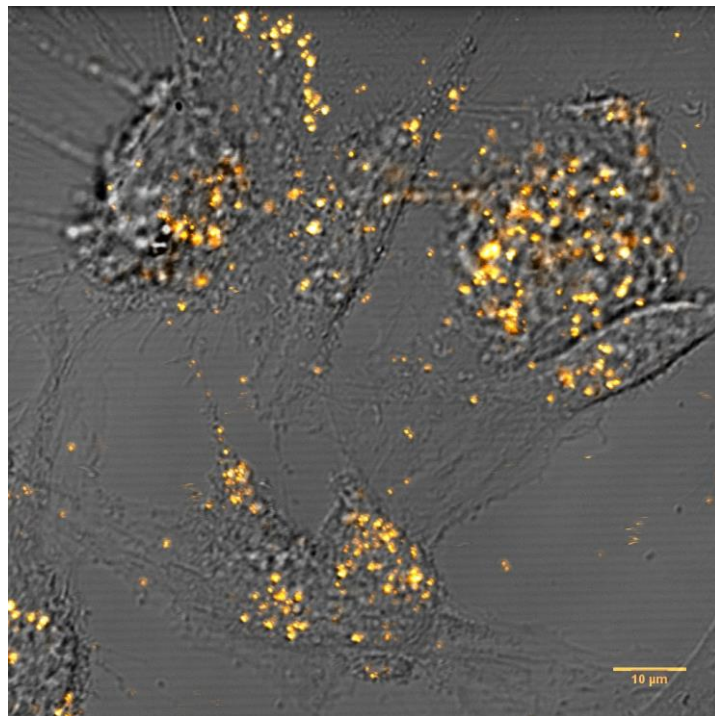


Figure G. Confocal image HMEC-1 cells incubated with MDMO-PPV NPs.

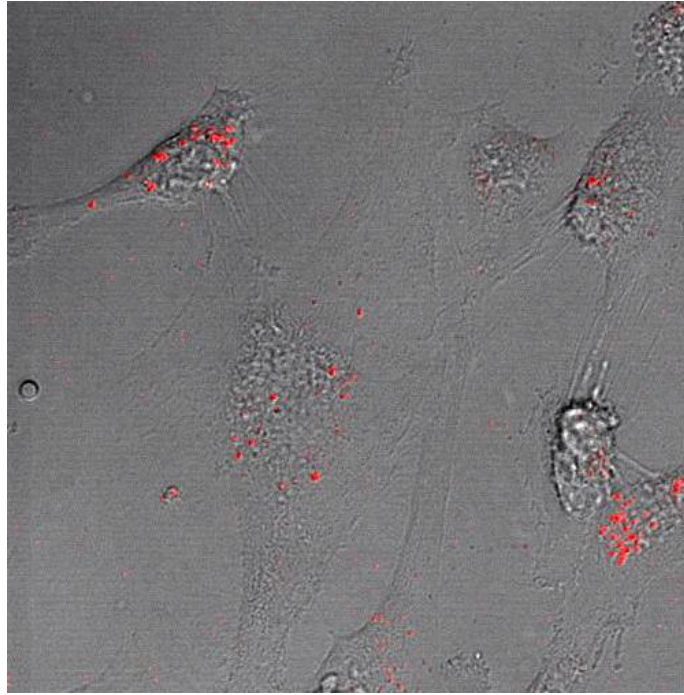


Figure H. Confocal image HMEC-1 cells incubated with MDMO-PPV/Magnetite NPs.

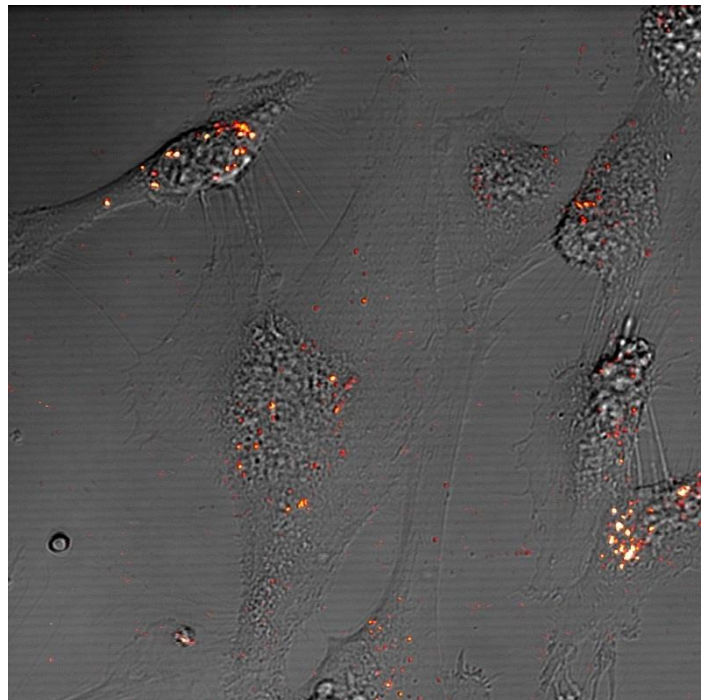


Figure I. Confocal image HMEC-1 cells incubated with MDMO-PPV/Magnetite NPs.

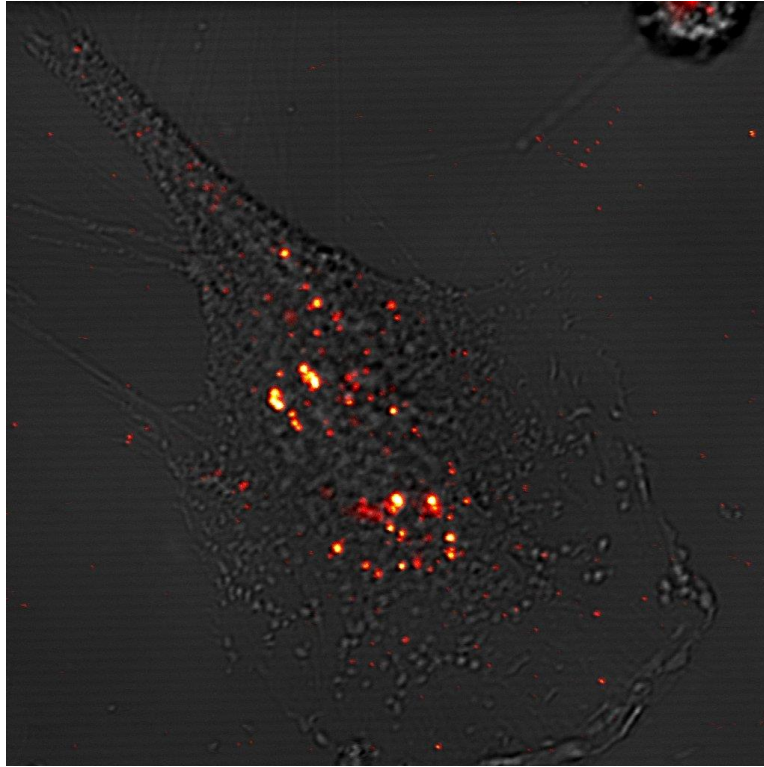


Figure J. Confocal image HMEC-1 cells incubated with MDMO-PPV/Magnetite NPs.

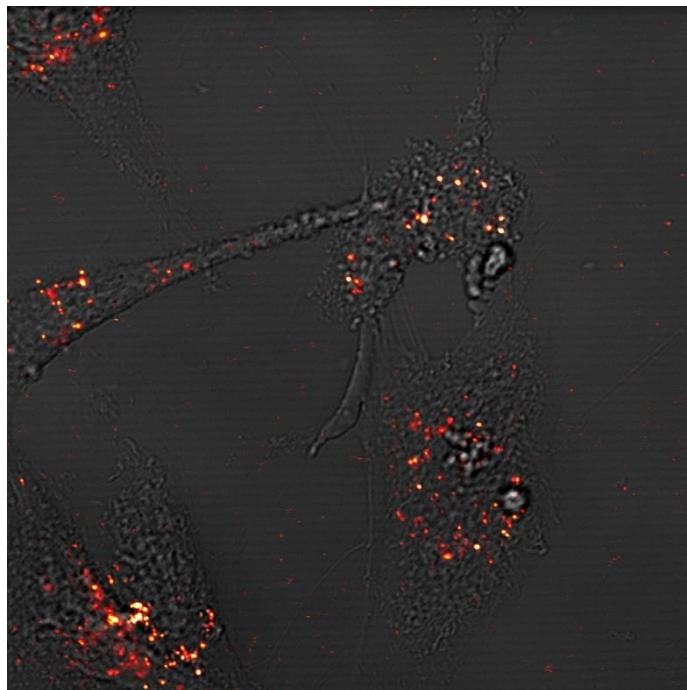


Figure K. Confocal image HMEC-1 cells incubated with MDMO-PPV/PLLA/Magnetite NPs.

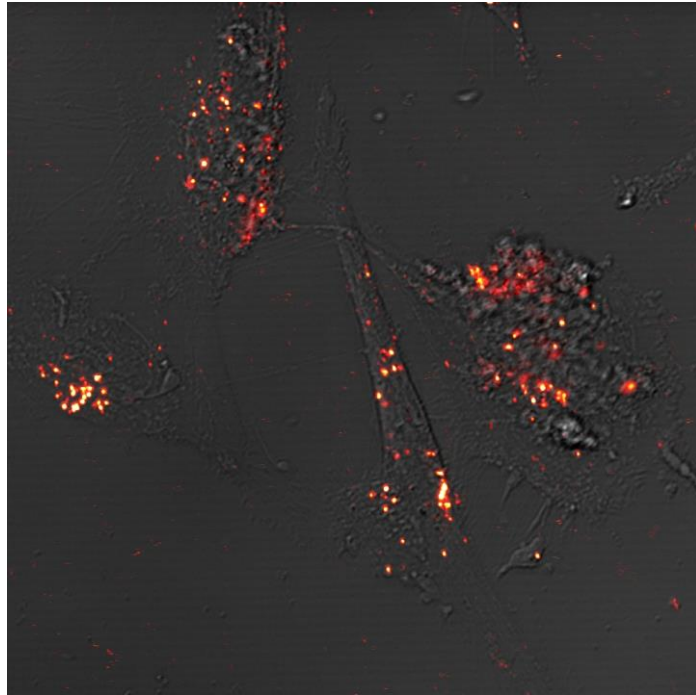


Figure L. Confocal image HMEC-1 cells incubated with MDMO-PPV/PLLA/Magnetite NPs.

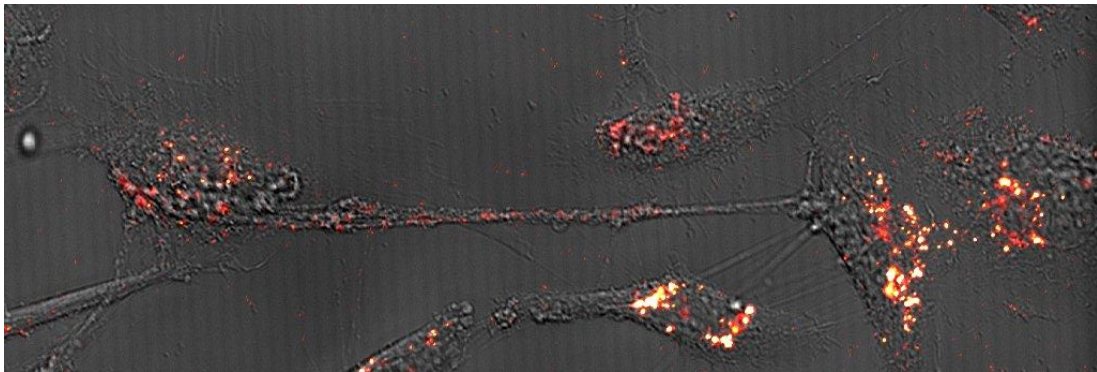


Figure M. Confocal image HMEC-1 cells incubated with MDMO-PPV/PLLA/Magnetite NPs.

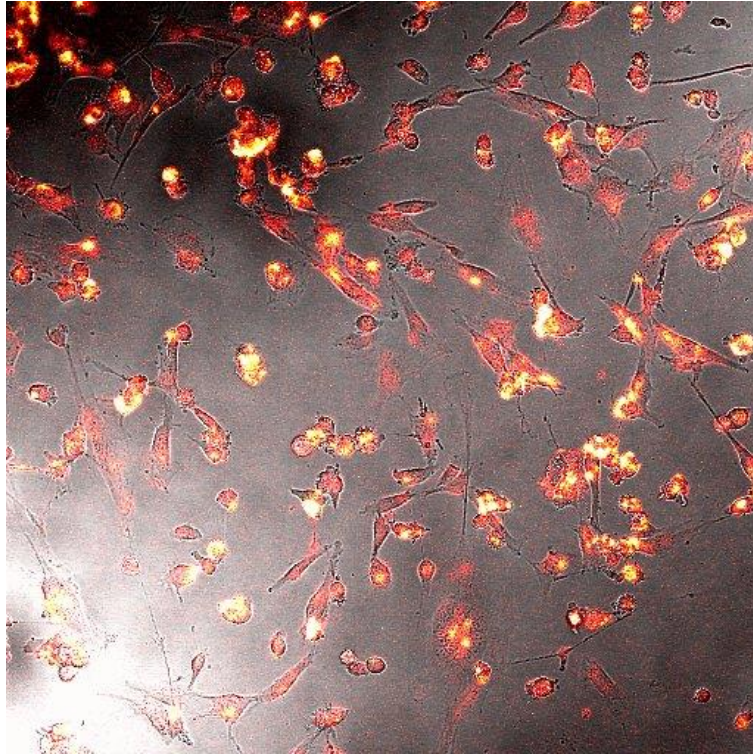


Figure N. Confocal image autofluorescence HMEC-1 cells incubated with PLLA/QDs NPs.

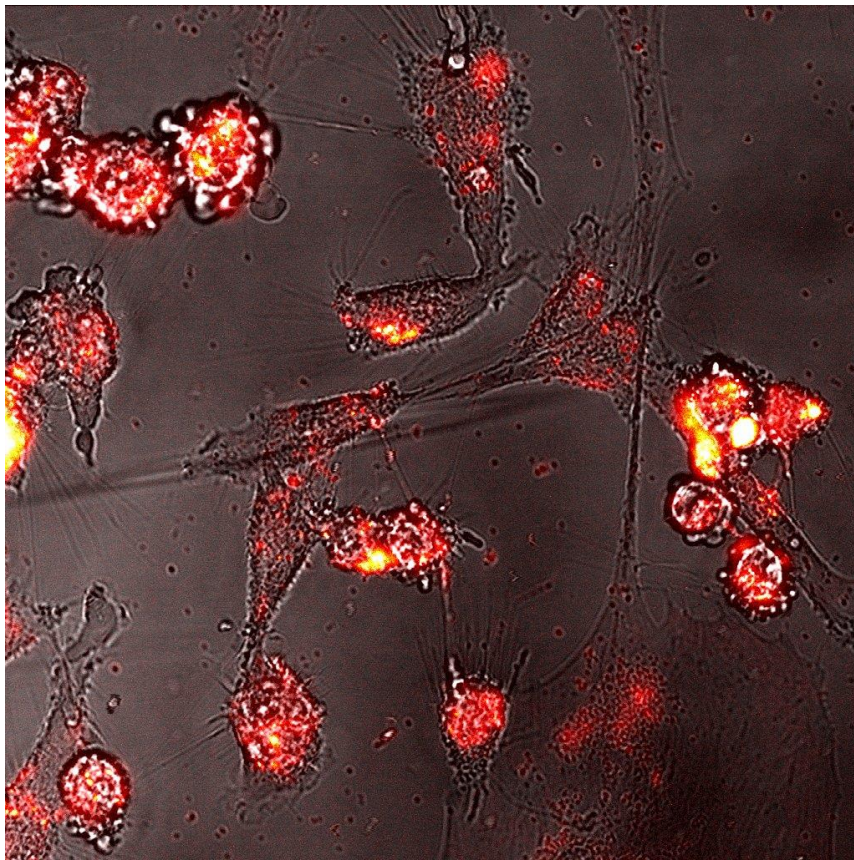


Figure O. Confocal image autofluorescence HMEC-1 cells incubated with PLLA/QDs NPs.

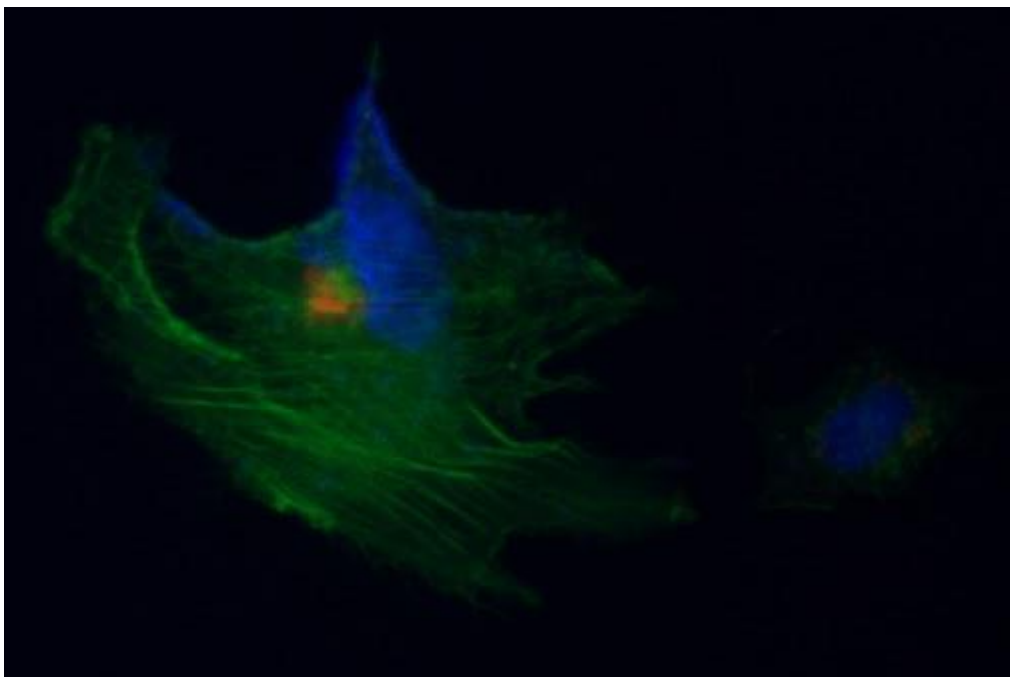


Figure P. Epifluorescence image HMEC-1 cells incubated with MDMO-PPV NPs.

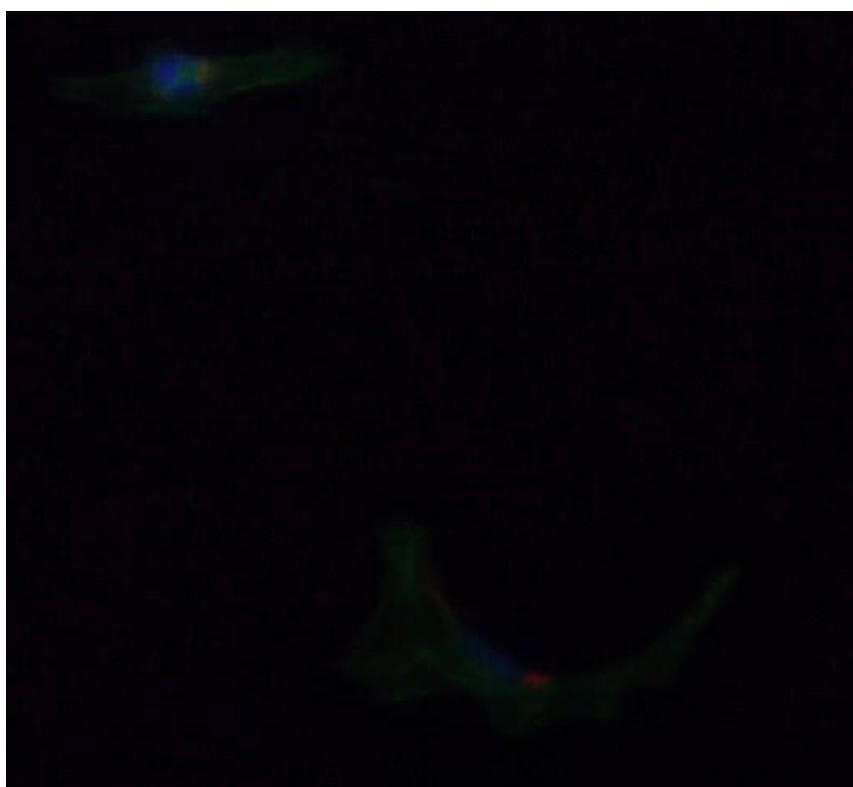


Figure Q. Epifluorescence image HMEC-1 cells incubated with MDMO-PPV/PLLA/Magnetite NPs.